

Review

# Perovskite@Graphene Nanohybrids for Breath Analysis: A Proof-of-Concept

Juan Casanova-Chafer <sup>1,\*</sup>, Rocio Garcia-Aboal <sup>2</sup>, Pedro Atienzar <sup>2</sup>, Carla Bittencourt <sup>3</sup> and Eduard Llobet <sup>1</sup>

<sup>1</sup> MINOS Research Group, Department of Electronics Engineering, Universitat Rovira i Virgili, 43007 Tarragona, Spain; eduard.llobet@urv.cat

<sup>2</sup> Instituto de Tecnología Química, CSIC-UPV, Universitat Politècnica de València, 46022 Valencia, Spain; rogarab@itq.upv.es (R.G.-A.); pedatcor@itq.upv.es (P.A.)

<sup>3</sup> Plasma-Surface Interaction Chemistry (ChIPS), Research Institute for Materials Science and Engineering, University of Mons, 7000 Mons, Belgium; carla.bittencourt@umons.ac.be

\* Correspondence: juan.casanova@urv.cat

**Abstract:** Nanohybrids comprising graphene loaded with perovskite nanocrystals have been demonstrated as a potential option for sensing applications. Specifically, their combination presents an interesting synergistic effect owing to greater sensitivity when bare graphene is decorated with perovskites. In addition, since the main drawback of perovskites is their instability towards ambient moisture, the hydrophobic properties of graphene can protect them, enabling their use for ambient monitoring, as previously reported. However not limited to this, the present work provides a proof-of-concept to likewise employ them in a potential application as breath analysis for the detection of health-related biomarkers. There is a growing demand for sensitive, non-invasive, miniaturized, and inexpensive devices able to detect specific gas molecules in human breath. Sensors gathering these requirements may be employed as a screening tool for reliable and fast detection of potential health issues. Moreover, perovskite@graphene nanohybrids present additional properties highly desirable as the capability to be operated at room temperature (i.e., reduced power consumption), reversible interaction with gases (i.e., reusability), and long-term stability. Within this perspective, the combination of both nanomaterials, perovskite nanocrystals and graphene, possibly includes the main requirements needed, being a promising option to be employed in the next generation of sensing devices.

**Keywords:** perovskite; graphene; gas sensor; breath analysis; biomarkers



**Citation:** Casanova-Chafer, J.; Garcia-Aboal, R.; Atienzar, P.; Bittencourt, C.; Llobet, E. Perovskite@Graphene Nanohybrids for Breath Analysis: A Proof-of-Concept. *Chemosensors* **2021**, *9*, 215. <https://doi.org/10.3390/chemosensors9080215>

Academic Editor: Ettore Massera

Received: 1 July 2021

Accepted: 5 August 2021

Published: 8 August 2021

**Publisher's Note:** MDPI stays neutral with regard to jurisdictional claims in published maps and institutional affiliations.



**Copyright:** © 2021 by the authors. Licensee MDPI, Basel, Switzerland. This article is an open access article distributed under the terms and conditions of the Creative Commons Attribution (CC BY) license (<https://creativecommons.org/licenses/by/4.0/>).

## 1. Introduction

Human breath is a complex matrix in which it is possible to find hundreds or even thousands of gas compounds [1]. Among this wide variety of molecules, some of them offer essential information about diseases or health disorders [2]. Noticeably, there are available completely reliable techniques such as computed tomography scan or blood analysis to detect some health issues, but they usually also are relatively expensive and time-consuming [3]. For that reason, during recent years, great research efforts have been focused on the development of non-invasive devices to perform fast and in situ analyses [4,5]. It is worth noting that these new approaches are not designed to replace the existing techniques; their conception is complementary, since these non-invasive techniques can act as a screening tool for the early-stage detection of health problems. In other words, new approaches such as the analysis of the human exhaled breath will enable point of care testing [6]. For instance, the presence of some volatile organic compounds (VOCs) such as benzene and toluene in breath can be indicative of lung cancer [7,8]. Even some infectious diseases such as tuberculosis can be detected through breath analysis [9]. As a consequence, there is a need for reliable devices able to analyze the exhaled breath, giving a new insight towards the early detection of health problems.

During recent years, chemical resistive (chemoresistive) sensors have been attracting a growing interest in front of other techniques such as gas chromatography coupled to mass spectrometry (GC–MS) and optical sensors. These techniques offer reliable results, being also capable of detecting trace levels of gas species [10]. However, some drawbacks are still a challenge, preventing their implementation in industrial applications for exhaled breath analysis [11]. For instance, GC–MS and optical sensors are usually costly and require trained personnel to operate, and further miniaturization is still-needed [12]. Conversely, in-field applications of chemoresistive sensors out of the laboratory are feasible due to their simplicity, easy miniaturization, and low-power consumption [13]. Moreover, chemoresistive devices offer outstanding properties as high sensitivity, straightforward readouts, and inexpensiveness owing to simple driving circuitry and facile fabrication [14], enabling a potential integration in commercial devices.

Nevertheless, the main issue that constitutes a significant barrier towards the commercial exploitation of chemoresistive devices is their poor selectivity. In other words, since very sensitive films can be developed to detect trace levels of a wide variety of gases, the design of nanomaterials able to distinguish certain compounds in a matrix is still a significant drawback. Some strategies have been proposed to overcome or at least mitigate this challenge, such as the use of sensor arrays combining different types of nanomaterials [15]. For instance, Y. Zhang and collaborators reported a gas sensor array comprising four devices based on  $\text{LaFeO}_3$  [16]. Moreover, these authors used silver as a cross-linker for grafting different functional monomers that acted as receptors of several gases such as benzene, ethanol, and acetone, among others. With that, despite the overlapped sensitivities obtained, some monomers were significantly more sensitive than others for specific gas molecules. This approach can pave the way to counteract the cross-selectivity of gas sensors with poor specificity. Nevertheless, in this case, an additional multivariate data analysis such as principal component analysis (PCA) is needed (Figure 1). Then, PCA outputs can be used to point out similarities and differences within the experimental data and reveal possible underlying patterns in high-dimensional sensing data [17]. However, the use of an array of sensors involves more expensive and complex devices, as well as additional data treatments and, therefore, more time-consuming analysis [18].

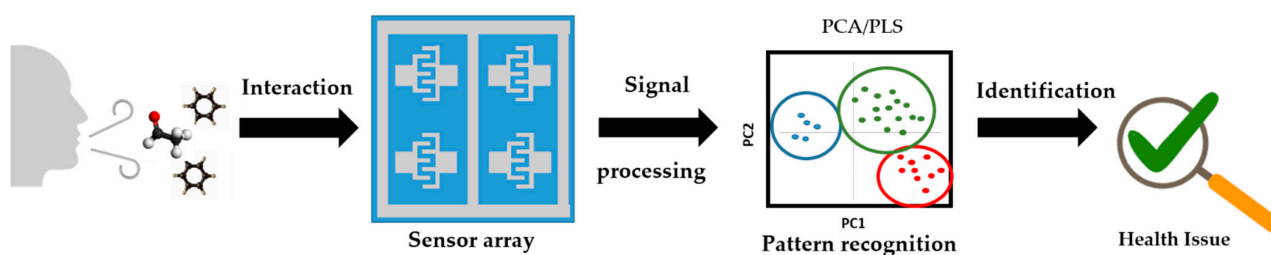


**Figure 1.** Scheme of the process to improve the selectivity issue. Biomarkers from human breath samples interact with different sensitive layers of the sensor array. Response features are treated by a dimensionality reduction or clustering step (e.g., principal component analysis, PCA) and a classification or regression step (e.g., partial least squares, PLS) may be used for identifying the presence of certain gas compounds associated with health problems.

To date, graphene-based gas sensors have been attracting large research interest for developing a new generation of nanoelectronics [19]. Many works have been mainly focused on ambient monitoring of atmospheric pollutants such as  $\text{NO}_2$  [20], volatile organic compounds (VOCs) [21],  $\text{H}_2\text{S}$  [22],  $\text{SO}_2$  [23],  $\text{CO}$  and  $\text{CO}_2$  [24,25],  $\text{NH}_3$  [26], and even chemical warfare agents [27]. Nevertheless, fewer works have centered on the use of graphene-based devices to detect biomarkers in exhaled breath [6] despite their outstanding properties. Graphene shows the ideally highest surface area to volume ratio due to its 2D configuration, in which all atoms can be exposed to their surroundings in atomically thin graphene [28]. In addition, some properties, such as low level of noise and high carrier density and mobility [29,30], make graphene an interesting candidate to be

employed in commercial devices. Additionally, the graphene capability to be operated at room temperature conditions for sensing applications leads to lower-consumption devices, simpler circuitry, and, as a consequence, better cost-effective chemoresistors. This fact is derived from the unnecessary implementation of heating elements that increase the working conditions of the sensitive films well-above the ambient temperature.

Nevertheless, it is worth noting that pristine graphene, meaning the  $sp^2$  carbon configuration, exhibits several issues towards its use in sensing applications. The main drawback is that pristine graphene presents chemical inertness [31], resulting in poor sensitivity and selectivity due to the low adsorption energies and small charge transfers, especially when is operated at room temperature [32]. It is worth noting that device configuration also has an essential role in sensing performance. For instance, Q. Li and collaborators demonstrated that the use of graphene contacting metallic electrodes (e.g., nickel) improves the sensitivity and response times in comparison to the bare graphene sheet resistance [33]. Additionally, other parameters such as thermal annealing can significantly change the graphene–metal contact resistance, resulting in different sensing performances [34]. Indeed, these graphene–metal contacts can be engineered for favoring the detection of specific gas species. For instance, C.L. Pereira and collaborators studied how  $H_2$  detection induces a doping near the graphene–metal heterojunction. Therefore, by changing the metal employed it is possible to control the electron transfer, resulting in significant resistance variations [35].

However, further modifications or functionalizations are usually needed to enhance the sensing properties of graphene-based devices. The most common strategies are graphene decoration with metal or metal oxide nanoparticles [36], plasma functionalization to promote the creation of structural defects [37], and the creation of nanocomposites with another type of material such as dichalcogenides [38] or polymers [39]. With those approaches, it is possible to some extent to improve sensing parameters such as sensitivity and response/recovery times. However, selectivity is not usually ameliorated to a very high extent, and additional problems can be derived from the use of these nanomaterials. For instance, to activate the electronic and chemical sensitization roles of metal nanoparticles or dichalcogenides, is often necessary to increase the operating temperature [30], compromising their low-power consumption and possibly lowering the device lifetime.

For that reason, in recent years, many researchers have explored a wide variety of new nanomaterials to complement graphene and improve the sensing performance. Among them, different perovskite compositions, especially those that do not involve the use of oxides, have emerged as attractive nanomaterials to be employed in sensing studies [40]. Indeed, their capability to operate at room temperature during the gas sensing has the same advantage as graphene-based sensors, enabling the development of simple and easy-to-use devices by their combination. In addition, perovskites show interesting properties from the sensing point of view, such as high reactivity, tunable bandgap, and long carrier lifetime [41]. The present work comprises the main strategies for functionalizing graphene and their combination with perovskites to develop sensitive films for the detection of gas compounds susceptible to be biomarkers in human exhaled breath.

## 2. Perovskites Compounds

### 2.1. Perovskite Structure

The main perovskite structure comprises the formula  $ABX_3$ , where A and B are cations of different sizes, while X corresponds to an anion. The crystalline structure is arranged in octahedra, in which every cation B is enclosed at the center of the octahedron and coordinated with 6 anions X that are located at the corners. Regarding cation A, this is coordinated with 12 anions, resulting in a cation A located at the center and surrounded by eight octahedra (Figure 2a). Thereby, this arrangement results in a cubic unit cell, where the cations A and B are located at the center and the corners of the unit cell, respectively, while the anion X occupies the edges of the unit cell (Figure 2b).

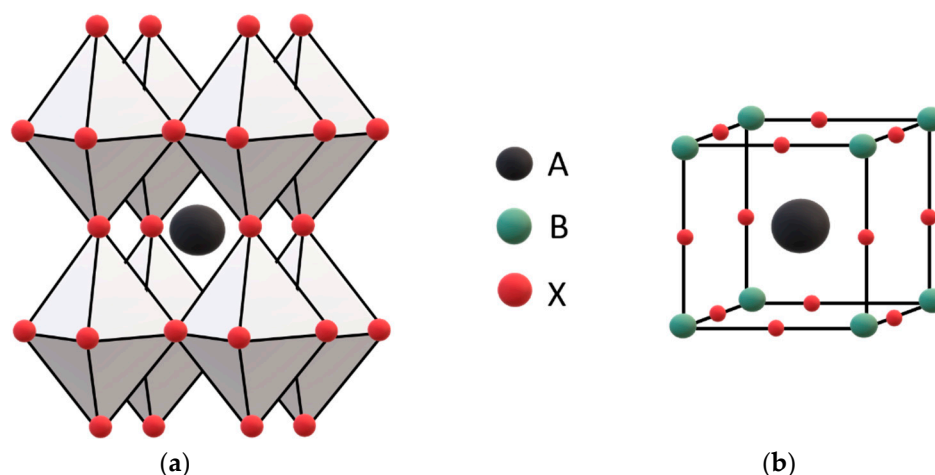


**Figure 2.** Perovskite arrangement in  $ABX_3$  structure: (a) 3D crystalline lattice; (b) unit cell of perovskite.

This structure confers high versatility to anion and/or cation substitutions, enabling the modulation of the physicochemical and sensing properties. Not limited to this, the large size difference in both cations present in the perovskite leads to a wide variety of dopant additions [42], allowing the modulation of key parameters, such as catalytic activity, to optimize the gas sensor performance for specific applications [43].

According to this, perovskites can be classified into two main categories: perovskite oxides ( $ABO_3$ ) when the anion X is oxygen, and halide perovskites ( $ABX_3$ ) where the anion X is usually a halogen, the most studied being bromine, iodine, and chlorine. Thereby, halide perovskites offer different electronic and physicochemical properties than their oxide counterparts. In addition, the cation A in halide perovskites can present both an inorganic (e.g., cesium and rubidium) or organic (e.g., methylammonium:  $CH_3NH_3^+$  and formamidinium:  $(NH_2)CH^+$ ) nature. Moreover, the metal cation B is usually lead or tin [44,45], but very recently new lead-free perovskites could be synthesized to decrease toxicity and open new possibilities to modulate the electronic and physicochemical properties [46]. Nevertheless, considering the different ionic radii of A, B, and X sites, the cubic structure can be distorted. According to Goldschmidt's tolerance factor ( $t$ ) [47], the undistorted cubic structure has values of  $0.8 < t < 1$ . However, values of  $t$  below 0.8 induce the distortion of the cubic structure because of octahedra tilting. As a result, different symmetries like orthorhombic, tetragonal, and monocyclic can be obtained. Conversely, values of  $t$  above 1 lead to hexagonal symmetries [48].

Despite this wide range of feasible perovskite compositions, they can also be synthesized in a variety of forms. Specifically, from zero- to three-dimensional perovskite nanostructures have been obtained (Figure 3). This is mainly possible by changing the size of the cation A located at the center of the unit cell (enclosed between the octahedra), leading to a modulation of the perovskite dimensionality [48]. In other words, a larger radius of cation A leads to greater distances between octahedra, resulting in lower dimensions. Thereby, their intrinsic properties and in consequence their sensing performance can be also modulated by changing the morphologies used [49,50]. Indeed, different perovskite nanostructures can be employed for the creation of hybrids with other nanomaterials, such as dichalcogenides, graphene, or metal oxides [51]. This outstanding versatility and these properties seem to fulfill the demanding requirements for the next generation of electronics, opening new perspectives to use perovskites in gas sensing devices.

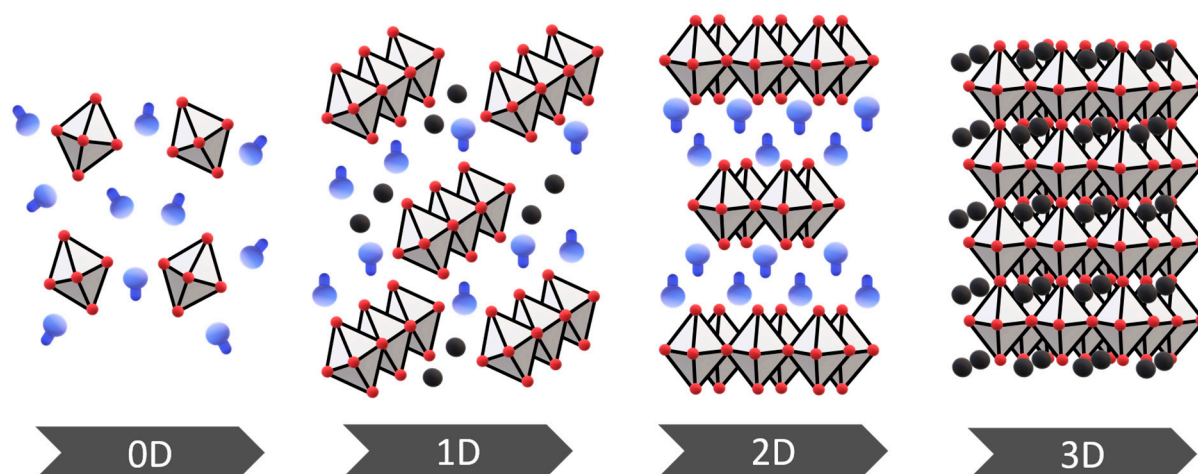


**Figure 3.** Schematic illustration of perovskite-related materials for different dimensionalities (Black: cation A; Red: anion X; Blue: cation A' with larger radius).

## 2.2. Perovskite Oxides

To date, inorganic perovskite oxides have been extensively used in gas sensing applications to detect a wide variety of compounds [52–55]. This configuration enables a rather good variability in perovskite compositions,  $\text{SrTiO}_3$ ,  $\text{LaFeO}_3$ , and  $\text{ZnSnO}_3$  [56–58], to cite some, being the most usually employed. As mentioned before, the change in the elements used and their nanostructure form can lead to different sensing properties. Moreover, these oxides can be used for the creation of hybrids with other nanomaterials. For instance, H. Zhang and J. Yi used  $\text{LaMnO}_3$  nanoparticles to decorate  $\text{ZnO}$  nanoflowers [59]. As a result, the detection of ethanol in the range of 10–200 ppm was enhanced 74% when the perovskite oxide was present in the sensitive film. However, as will be discussed later, the use of oxides shows a significant drawback, which is the high operating temperature needed. In this case,  $\text{LaMnO}_3@ZnO$  samples require 300 °C. Regarding the nanohybrids comprising perovskite oxides and graphene, few works reported feasible applications, such as gas sensors [60] or solar cells [61], probably owing to the poor alignment between these two nanomaterials, since the operating temperatures are significantly different.

Perovskite oxides show interesting properties such as high ferroelectricity [62], and structural and morphological stability [63], extending their potential operational life and therefore their reliability in sensing devices. This type of nanomaterial also shows high catalytic activity due to the large concentration of oxygen vacancies, chemisorbed oxygen from the air, and defective sites on the surface [64]. However, this high sensitivity due to their catalytic activity results in poor specificity (i.e., selectivity) towards gas molecules. In addition, to activate their catalytic properties, rather high operating temperatures are usually needed [65]. It is worth noting that one of the main advantages of the perovskite oxides is their thermal stability, requiring high temperatures for their melting and decomposition. However, these operating conditions at hundreds of degrees centigrade [66,67] result in high device power-consumption, a more complex circuitry due to the presence of heating elements, and therefore higher costs. This fact can constitute an important barrier to their adoption in commercial devices.

Regarding the lack of selectivity, this is an unsolved issue despite the great research efforts done. Overall, the sensing mechanism of bare perovskite oxides is based on the interaction of gas molecules with chemisorbed atmospheric oxygen adsorbed on the perovskite oxide surface. Thus, adsorbed oxygen species capture electrons from the nanomaterial, increasing the hole concentration. Hence, when gas compounds interact with the chemisorbed oxygen, the electrons are released and recombined with holes. Additionally, it is worth noting that gas compounds can interact with oxygen vacancies and defective

sites on the perovskite oxide surface. However, these mechanisms are rather general, offering poor specificity towards gas molecules.

One strategy designed to ameliorate to some extent the selectivity of perovskite oxide-based gas sensors is their doping with other elements [68–70]. For instance, E. Cao and collaborators developed a chemoresistor based on Cl-doped LaFeO<sub>3</sub> for ethanol sensing [71]. The sensing response was significantly enhanced when the perovskite oxide was doped with chlorine. This better sensing performance is attributed to the replacement of adsorbed oxygen by chlorine dopant, increasing the charge transfer between gas molecules and doping elements. However, not limited to this, a few years later, Cl-doped LaFeO<sub>3</sub> perovskites were further modified with Au atoms [72], increasing even more the sensitivity to ethanol. Since this strategy is perfectly reasonable to improve the sensing performance, each additional step for modifying the perovskite oxides increases the complexity of their synthesis and their cost of production. Despite these better sensing responses, it is worth noting that the selectivity issue is still a challenge, preventing their use in commercial applications.

Another common element used for doping perovskite oxides is silver. Several works reported their use for obtaining Ag@ZnSnO<sub>3</sub> [73] and Ag@LaFeO<sub>3</sub> [74] for acetone and formaldehyde gas sensing, respectively. In both cases, the silver-doped perovskites show higher sensing responses (up to 3-fold) than their bare perovskite oxides. Nevertheless, cross-sensitivity should be further improved to be able to discriminate certain gas compounds, and the operating temperatures should be lowered even in the presence of these doping elements. In this regard, Y. Tie and collaborators demonstrated that by doping BiFeO<sub>3</sub> hollow nanofibers with Pr, the optimum operating temperature for detecting some gases such as formaldehyde can be lowered to some extent [75].

An additional issue related to the use of perovskite oxides is their dependence of the water vapor levels. This phenomenon can be an opportunity for the ambient monitoring applications, in which doped perovskite oxides like Mg@LaFeO<sub>3</sub> [76] and Sm@LaMnO<sub>3</sub> [77] were employed as humidity sensors, taking advantage of this dependence. However, considering the high content of water vapor in exhaled breath, this probably prevented the ability to detect biomarker molecules in the same matrix due to the significant cross-sensitivity [78]. For that reason, the approach proposed by Q. Chen, in which gold nanoparticles inhibit the moisture influence [79], can have a large impact on the next generation of sensing devices for exhaled breath applications. Specifically, these authors decorated In-doped ZnSnO<sub>3</sub> perovskites with Au nanoparticles. As a result, the sensor responses to acetone were kept almost changeless against different levels of ambient moisture. Even more, the response and recovery times were further lowered, but as usual in this type of nanomaterial, relatively high operating temperatures (200 °C) were still required.

### 2.3. Halide Perovskites

Halide perovskites, classified as inorganic and organic in nature, depending on the cation A employed in the ABX<sub>3</sub> structure, offer an extreme variety of potential compositions. During recent years, this type of nanomaterial has emerged as a thriving research field, attracting the attention of many works centered on studying their different properties according to the anions and cations used. In fact, their effective use in solar cells [80] and photocatalytic [81,82] applications has been extensively studied and demonstrated. However, despite their interesting properties from the sensing point of view such as tunable bandgap, high electron/hole mobility, long carrier lifetimes, and large adsorption coefficients [41], fewer works use them as gas sensors.

Halide perovskites show some intrinsic properties that make them ideal candidates for the next generation of gas sensing devices. For instance, this nanomaterial is usually able to operate at room temperature [83], leading to reduced power consumption and inexpensive devices owing to their simpler circuitry. Moreover, many halide perovskites can be synthesized via solution processing methods, involving facile and low-cost synthesis [84]. Some works reported the use of halide perovskite thin films as gas sensors for different

target analytes such as NO<sub>2</sub> [85], NH<sub>3</sub>, [86], H<sub>2</sub> [87], ozone [88], and acetone [89], to cite some. In this regard, halide perovskites can also be employed to detect gas compounds susceptible to be biomarkers, but several parameters should be further improved. For instance, A. Nuraini and I. Oh reported a thin film of MAPbI<sub>3</sub> for detecting ethanol [90], but the concentration tested was 10,000 ppm, showing an LOD of 1300 ppm, far from those levels needed in practical uses. Another example is the work done by W. Jiao [91], in which a thin film of lead halide perovskite was used for detecting ammonia gas, but this compound showed an irreversible reaction with the sensitivity film, resulting in the lowering of the sensing performance and the degradation of the nanomaterial.

Therefore, in combination with further optimization of halide perovskite gas sensors, probably more research efforts are needed to couple them with other nanomaterials. To date, few works have engineered this type of perovskite to create nanocomposites, such as their doping with atoms of other natures [92] or the introduction of organic molecules into the halide perovskite lattice [93]. Another interesting alternative for optimizing gas sensor properties can be the use of UV or visible light activation to take advantage of the outstanding absorption coefficient properties of halide perovskites. With that, it would be possible to enhance the sensing performance because the light activation induces the formation of electron–hole pairs in halide perovskites, increasing their reactivity (i.e., sensitivity) towards gas molecules located in their surroundings.

Nevertheless, halide perovskite-based gas sensors present significant drawbacks that are still unsolved. The main one is related to their fast degradation in the presence of ambient moisture [94]. Water molecules considerably reduce their stability, limiting their potential implementation in commercial applications. Moreover, some changes in the temperature or pressure can disrupt the halide perovskite crystallinity [95], being a challenge that still has to be overcome.

### 3. Perovskite@Graphene Nanohybrids

#### 3.1. Graphene Functionalization

The reported properties of graphene provide a myriad of possibilities for applications in different technological areas such as electronics, energy storage and conversion, and particularly property enhancement in hybrid materials. However, its low dispersibility in both organic and inorganic solvents prevents its optimal combination with different nanomaterials, which is a key problem for graphene technologies. Therefore, the modification of graphene to tailor its solubility is critical for varied applications. Basically, graphene can be modified with covalent and noncovalent methods. Non-covalent methods include  $\pi$ – $\pi$  stacking interactions, electrostatic interaction, hydrogen bonding, coordination bonds, and van der Waals force [96–98]. These methods are considered to preserve most of the graphene properties, though the interaction between the added functional groups and the graphene surface are relatively weak; hence, it is not appropriate for applications where strong interactions are required. Conversely, in the covalent modification methods, strong interactions between graphene and the added functional groups are present; therefore, the graphene pristine structure is normally disrupted, leading to inferior electrical conductivity and mechanical properties, however promoting a better quality hybrid material due to better dispersion and improved interaction among different materials that compose the hybrid material [99,100].

Covalent modifications are obtained via disruption of the conjugation of graphene sheets [96]; depending on the amount of defects created, the graphene natural conductivity can be strongly negatively affected. This type of modification is applicable when total preservation of graphene's natural conductivity is not necessary, such as in tuning of graphene's solubility, anti-bacterial activity, or surface chemical reactivity. Covalent modifications can also be obtained via doping heteroatoms onto the graphene lattice [101–103]. Furthermore, for graphene produced via the oxidation–reduction method, the partial reduction results in oxygen-containing functionalities grafted at the graphene surface, also permitting covalent modifications [104]. Oxidation and reduction processing is a facile method to tune

graphene properties by controlling the number of grafted oxo-groups and lattice defects. Therefore, methods that allow the reduction degree of GO to be tuned have attracted extensive attention, as controlled reduction removes the excess of oxygen-containing groups and different atomic-scale lattice defects and also recovers the conjugated network of the graphitic lattice [105].

Different methods can be used for GO reduction such as thermal annealing [106], microwave and photo irradiation [107–109], chemical reduction [110,111], and electrochemical [112] and solvothermal reduction [113,114]. Among these methods, thermal annealing, chemical reduction, and microwave irradiation are the most commonly used. For example, N.J. Song and collaborators [115] prepared thin films of GO with tailored conductivity and mechanical performance by changing thermal annealing temperatures. These authors showed that for increasing temperature, the removal of oxygen-containing functional groups increases with simultaneous conversion from  $sp^3$  to  $sp^2$  carbon bonding in the hexagonal carbon lattice. At the end of the thermal annealing near 1000 °C, the material exhibits high thermal conductivity of ca.  $1043.5 \text{ Wm}^{-1}\text{K}^{-1}$ , and excellent mechanical stiffness and flexibility with a high tensile strength (13.62 MPa) and Young's modulus (2.31 GPa). M. Feng and collaborators [116] reported on the effect of different reducing agents on the de-oxygenation and restoration of  $\pi$ - $\pi$  conjugation of graphene oxides (GO). These authors compared the reduction using basic (sodium hydroxide (NaOH), sodium borohydride ( $\text{NaBH}_4$ ), hydrazine hydrate, and  $\text{NaBH}_4$  and hydrazine hydrate) and neutral (superheated  $\text{H}_2\text{O}$ ) reducing agents. The treatment with hydrazine hydrate was the most effective for the reduction of GO.  $\text{NaBH}_4$  and superheated  $\text{H}_2\text{O}$  were the next best performing reducing agents, and NaOH was the least efficient. However, by treating GO powders in a commercial microwave-assisted oven, reduced GO can be readily obtained within 1 min in ambient conditions, which greatly improved the graphene preparation efficiency [117].

### 3.2. Development and Characterization of Perovskite@Graphene Nanohybrids

In recent years, the resurgence of graphene-related materials in chemical sensing and photovoltaics followed the emergence of metal halide perovskite solar cells [118,119]. The use of graphene oxide, reduced graphene oxide, or functionalized graphene within metal halide perovskite solar cells has been reported as an optimal approach to tackle the main challenges, such as enhancement of photovoltaic performance and stability, controllable thin film growth and deposition, scalability, and cost [118,120,121]. For instance, M. Li and collaborators [121] reported that addition of oxo-functionalized graphene/dodecylamine suppressed the ion migration in perovskite solar cells. These authors showed that the chemically functionalized graphene flakes wrapped the perovskite crystal, isolating them and thus reducing ion migration inside the active layer [121–123]. Within the perspective of using halide perovskite as an active material in gas sensing, J. Casanova-Chafer and collaborators showed that graphene has a decisive role in the stability of the sensing layer and its performance towards the fast detection of volatile organic compounds [119].

Regarding the perovskite metal oxides, the ambient moisture tends to form hydroxyl ions at the nanomaterial surface [124]. In the case of halide perovskites, water molecules induce the distortion of the perovskite lattice, resulting in a probable degradation [125]. For instance, it was reported that  $\text{CH}_3\text{NH}_3\text{PbI}_3$  perovskite is degraded into  $\text{CH}_3\text{NH}_3\text{I}$  and  $\text{PbI}_2$  in the presence of ambient moisture [126]. It is worth noting that raising the temperature may partially revert these changes and enable the crystalline halide perovskite to be obtained upon removal of water molecules [127]. Nevertheless, this strategy does not seem reliable in industrial uses, and considering the presence of variable moisture levels in the atmosphere, the use of perovskites in commercial applications is in truth challenging.

To date, despite the significant research efforts done to improve perovskite stability against ambient moisture, there are not many feasible alternatives yet. However, a breakthrough has consisted of using lead halide perovskites nanocrystals to decorate graphene [119,128], avoiding perovskite degradation even in the long-term. The reason

behind the graphene loading with halide perovskite is based on the high graphene hydrophobicity, protecting perovskite degradation against the effect of ambient moisture. In this regard, the main goal is to obtain gas sensors using perovskites that are reliable for ambient monitoring and exhaled breath analysis, in which significant and variable water contents are present. Few works already reported the feasibility and benefits of developing perovskite–graphene nanocomposites in solar cell applications [129,130]. However, their implementation in the gas sensing research field is still exploitable.

Moreover, halide perovskites usually show deficient temperature stability, resulting in their degradation or at least changes in the phase transitions (e.g., from cubic to tetragonal or orthorhombic) that are lowering their properties [131]. This fact constitutes a significant problem, since even moderate temperatures near 150 °C may degrade the perovskites [132]. Therefore, room temperature working conditions are desirable from the sensing point of view, being translated into lower power-consumption and simpler circuitry. Moreover, it is interesting for the stability of the perovskites, resulting in a longer operation life. Considering this, the graphene capability to be operated at ambient temperature creates a synergy effect, in which the poor sensitivity of graphene can be ameliorated by the perovskites, while the instability of perovskites against ambient moisture can be tackled thanks to the hydrophobicity of graphene.

Specifically, we synthesized several metal halide perovskite nanocrystals for decorating graphene nanoplatelets. For better comparison, all graphene samples were decorated by using the same experimental conditions, and similar procedures were followed to synthesize the different perovskite compositions. In that way, the comparison of several samples with some changes in their compositions was feasible. Figure 4a depicts a high-resolution transmission electron microscopy (HR-TEM) image of the bare graphene. Overall, it can be appreciated that graphene layers presented lengths of a few hundred nanometers, while several layers were stacked, showing distances of about 2.4 Å. Figure 4b shows a field emission scanning microscope (FESEM) image of the deposited bare graphene onto the substrates. A porous surface can be observed, which usually confers interesting sensing performance. The easy and inexpensive methods followed for synthesizing the halide perovskite nanocrystals result in highly crystalline samples with an average diameter ranging from 6 to 8 nm (Figure 4c). Finally, Figure 4d shows the resulting hybrid nanomaterial, where graphene (black background) is quite homogeneous, decorated with the perovskite nanocrystals (bright spots). In brief, lead halide perovskite nanocrystals were supported on liquid-phase exfoliated (LPE) graphene, which is an interesting preparation method given its low cost [133].

### 3.3. Gas Detection

Casanova-Cháfer et al.'s first approach [128] was loading graphene with methylammonium (MA) bromide perovskite (MAPbBr<sub>3</sub>) nanocrystals for the detection of pollutants in the atmosphere. The short- or long-term exposition to these gases may have a hazardous effect on human health. In this regard, toxic gases such as NO<sub>2</sub> and NH<sub>3</sub> were detected at ppb and ppm levels, respectively. Indeed, the limits of detection (LOD) were situated below the threshold limit values (TLV), offering higher sensitivities (up to 3-fold) when graphene was decorated with perovskite nanocrystals than their bare graphene counterparts (Figure 5a). The nanohybrid developed showed higher sensing responses than perovskite thin films-based sensors [85,89], demonstrating the outstanding sensing performance of this perovskite–graphene implementation. Not limited to this, a second approach [119] was conducted by loading graphene with different perovskite nanocrystals. In particular, the role of different anions and cations was elucidated by preparing six compositions. Considering the ABX<sub>3</sub> perovskite structure, three cations A (methylammonium, MA (CH<sub>3</sub>NH<sub>3</sub><sup>+</sup>); formamidinium, FA ((NH<sub>2</sub>)<sub>2</sub>CH<sup>+</sup>); cesium (Cs<sup>+</sup>)), and three halide anions X (Cl<sup>−</sup>, Br<sup>−</sup>, and I<sup>−</sup>) were studied. Trace levels of aromatic VOCs such as benzene and toluene gases were measured (Figure 5b), offering stable, reproducible, and sensitive sensing readouts. These compounds are associated with several health issues,

such as sub-clinical lung cancer, when present in exhaled breath [7]; therefore, the use of perovskites opens new possibilities to develop sensing devices for biomarker detection. It is worth noting that when bare graphene was exposed to VOCs it was not possible to distinguish the resistance variation from the noise level. As a consequence, the sensing responses obtained could be attributed to the effect of the halide perovskites. In other words, perovskite nanocrystals act as chemical receptors, while graphene mainly acts as a charge conductor. Furthermore, significant differences in the sensing performance can be observed by changing the perovskite composition. Experimental results showed that MA cation presents higher sensitivities than FA and Cs (Figure 5c), while  $\text{Br}^-$  anions also offer better sensing responses than  $\text{Cl}^-$  and  $\text{I}^-$  (Figure 5d).

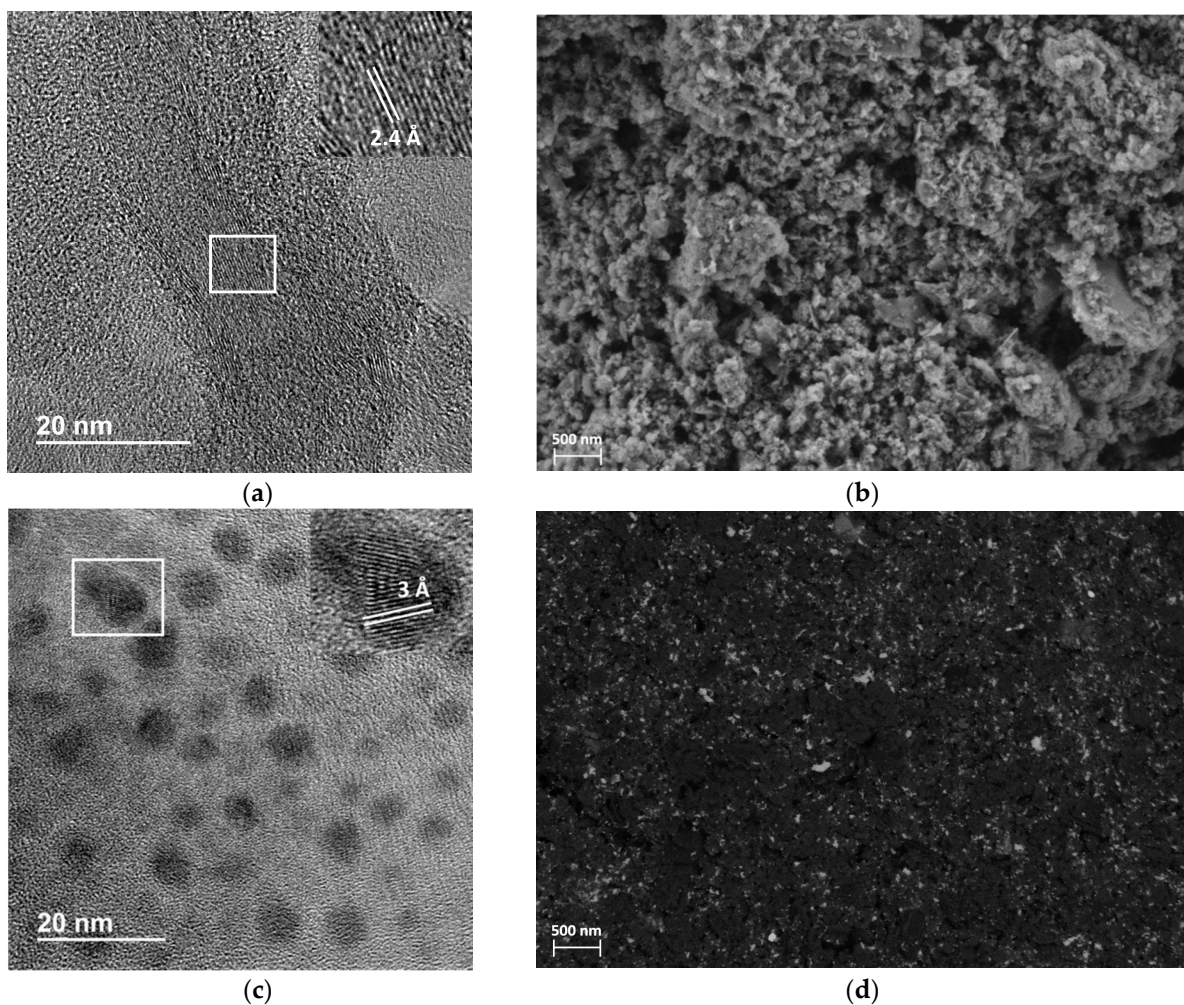


**Figure 4.** (a) HR-TEM image showing the typical layer size of the bare graphene used. (b) FESEM image showing the surface of the bare graphene. (c) HR-TEM image showing an example of the lead halide nanocrystals synthesized ( $\text{MAPbBr}_{2.5}\text{I}_{0.5}$ ), with interplanar distance of 3 Angstrom. (d) Example of FESEM image obtained via back-scattered electron (BSE) detector for  $\text{MAPbBr}_3$ . The black background corresponds to graphene, while bright spots denote the presence of perovskite nanocrystals.

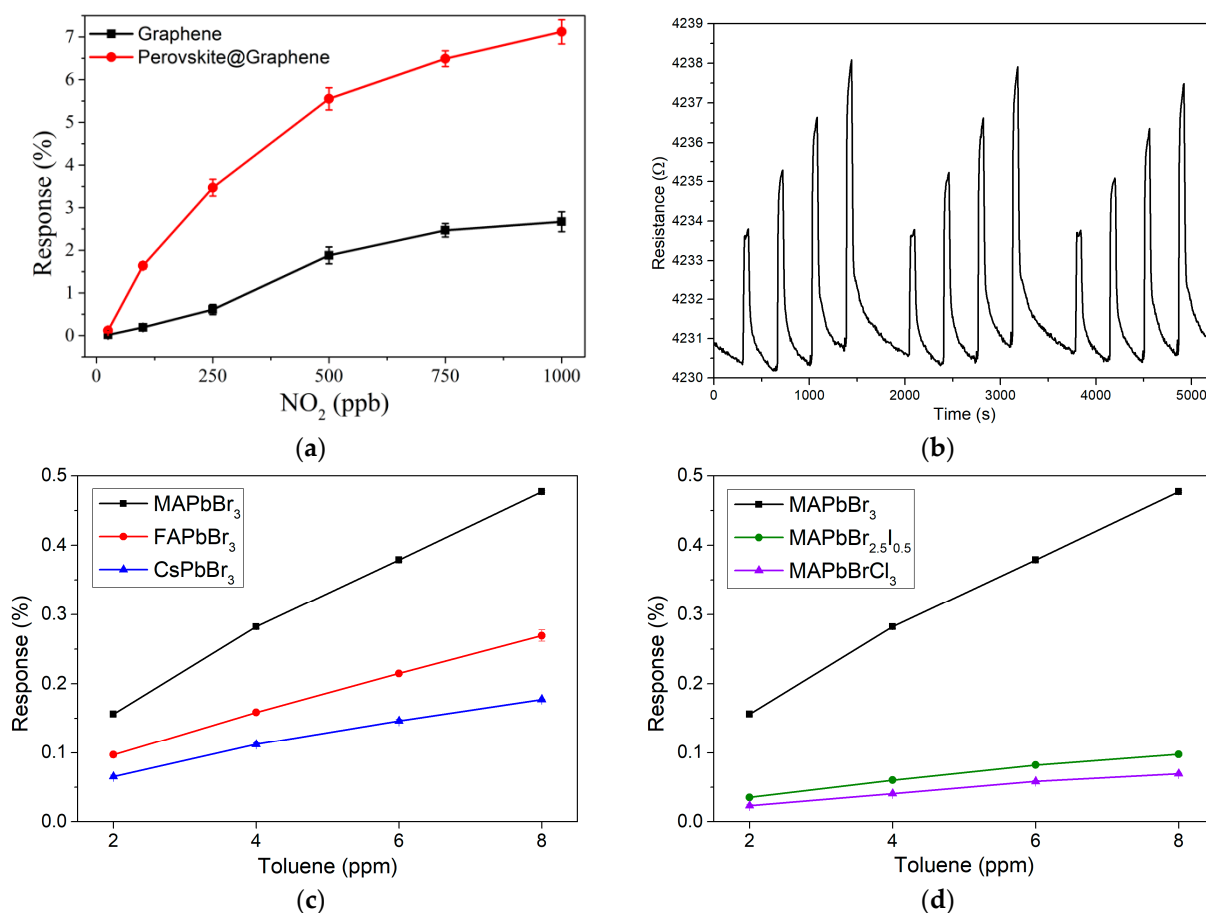


**Figure 5.** (a) Comparison of calibration curves obtained for bare and perovskite-decorated graphene detecting NO<sub>2</sub>. Reproduced from *Sensors MDPI* 2019, 19 (20), 4563. (b) Example of the dynamic responses to 2, 4, 6, and 8 ppm of benzene during three cycles by using graphene decorated with MaPbBr<sub>3</sub> nanocrystals. Example of the calibration curves obtained for detecting toluene using lead halide perovskite with different cation (c) and anion (d) compositions. *Chem. Commun.*, 2020, 56, 8956–8959. Reproduced by permission of The Royal Society of Chemistry (RSC).

It is understandable that graphene loaded with perovskite nanocrystals tends to show higher gas sensing responses than the bare carbon nanomaterial. Overall, the graphene employed shows a relatively small concentration of oxygen-containing groups (<10%). Nevertheless, these functional groups, such as carbonyl, hydroxyl, or ether, increase the hole transport capacity due to the shifting of the Fermi level towards the valence band and also by increasing the work function [134]. In this regard, for a well-known p-type semiconductor such as graphene, exposure to electron-withdrawing (e.g., NO<sub>2</sub>) or electron-donating (e.g., NH<sub>3</sub>) gases leads to a decrease and increase of the sensor resistance, respectively. This is because adsorbed gas compounds at the surface induce changes in the local carrier concentration with carbonaceous defects and oxygenated-functional groups grafted on the graphene layers [96]. However, the sensing responses for bare graphene samples are rather poor, especially if gas measurements are conducted at room temperature.

For that reason, considering the high reactivity of halide perovskites, their mere presence decorating graphene tends to show better sensing performance for a wide variety of gases at room temperature. It is worth noting that perovskites are ambipolar charge transporters [83], which means that they can act as an p- or n-type semiconductor depending on the interaction between the nano hybrids and the nature of the analyte. Indeed, the halide perovskites developed present surface trap sites acting as reactive sites for the target gas compounds. Specifically, a net positive charge is formed at the perovskite surface due to the loss of the halide and the undercoordination of the lead atom, promoting their sensitivity to gases. Thereby, once the sensitive films are exposed to the gases (Figure 6),

perovskites tend to separate electron–hole pairs, in which an interface is created between graphene and perovskite. As a result, an excess of positive (holes) and negative (electrons) charges are generated at the nanocrystals for electron-withdrawing and electron-donating gases, respectively. The excess of charge generated at the perovskite is transferred to the graphene [135], which is the dominant carrier transport nanomaterial, explaining the p-type behavior of the sensitive film. As a consequence, the sensing response to both types of gases can be improved when perovskite nanocrystals are decorating graphene sheets.

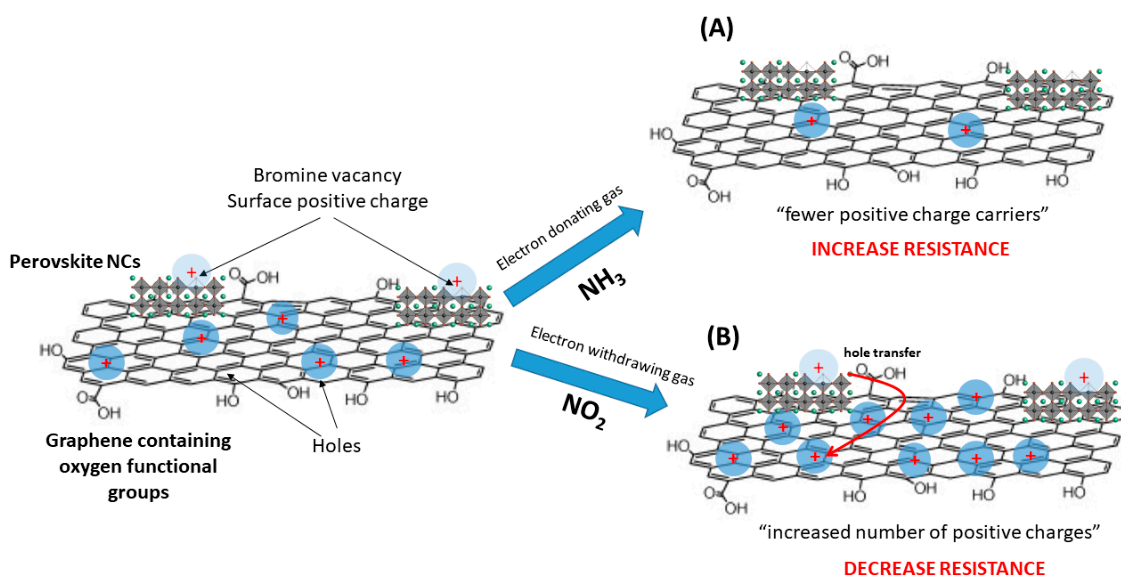


**Figure 6.** Synoptic illustration of the sensing mechanisms for graphene loaded with perovskite nanocrystals. (A) When halides perovskites interact with electron-donor gas, an excess of positive charges is neutralized at the defective perovskite surface, resulting in a decrease of the local hole concentration of the p-type graphene, and thereby the resistance increases. (B) When halide perovskites interact with electron-acceptor gas, positive charges are formed at the nanocrystals, being transferred to the graphene. As a result, the resistance decreases. *Reproduced from Sensors MDPI 2019, 19 (20), 4563.*

Nevertheless, it is important to point out that different  $ABX_3$  compositions offer differentiated sensing performances. According to Figure 5c,d, the perovskite  $MAPbBr_3$  shows better results than other anions and cations. This is probably derived from the relative energy level positions (band structure) and trap defect concentrations at the nanocrystal surfaces. According to the cation-substituted compositions, MA, which offered the higher gas sensing responses, leads to a better energy-level alignment with the graphene work function than do FA and Cs cations (Figure 7a). As a result, more effective hole extraction when detecting electron-donor gases like benzene and toluene can occur. In addition, the density of surface trap sites from under-coordinated Pb ions may also have a key role in the interaction with gas compounds. Thereby, since aromatic compounds can passivate the surface of the nanocrystals [136], it might be foreseen that  $MAPbBr_3$  presents a higher density of trap sites than  $FAPbBr_3$  and  $CsPbBr_3$ , especially considering that  $MAPbBr_3$  shows lower photoluminescence quantum yield than other perovskites tested [137]. Indeed, structural defects and vacancies may act as carrier traps quenching the photoluminescence [138], denoting a larger density of trap sites in  $MAPbBr_3$ , and therefore a higher number of available sites to react with gas compounds.

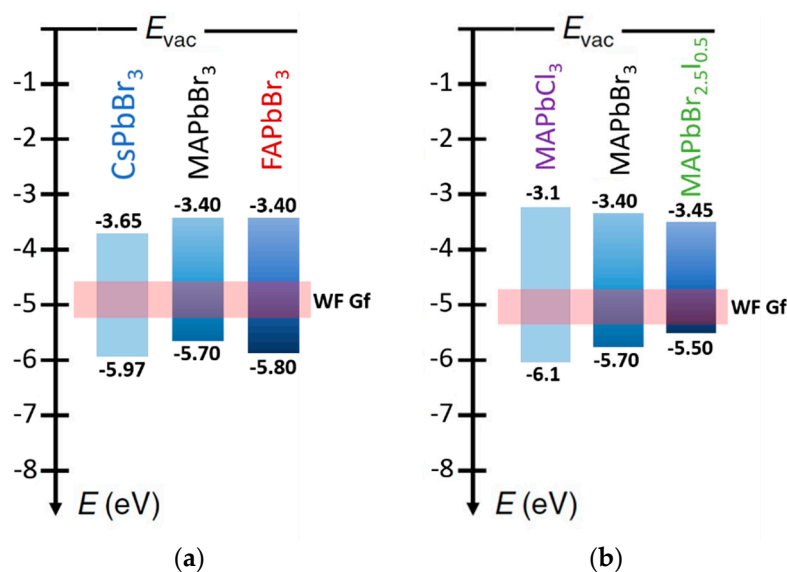


**Figure 7.** Band structure diagrams of different cation (a) and anion (b) halide perovskite compositions, and their comparison with the graphene flakes (GF) work function (WF). *Chem. Commun.*, 2020, 56, 8956–8959. Reproduced by permission of The Royal Society of Chemistry (RSC).

Regarding the halide anion influence on the sensing performance, experimentally the perovskite MAPbBr<sub>3</sub> led to better sensing results than Cl<sup>−</sup> and I<sup>−</sup>. However, the sample containing iodine (MAPbBr<sub>2.5</sub>I<sub>0.5</sub>) presents better energy-alignment with graphene (Figure 7b). This means that probably more parameters have an essential role to detect VOCs. For instance, it was reported that different halides show significant variations in carrier mobility, demonstrating that MAPbBr<sub>3</sub> and MAPbI<sub>3</sub> preferentially exhibit unipolar and ambipolar behavior, respectively. As a consequence, the excess of positive charges generated at MAPbBr<sub>3</sub> upon their interaction with benzene and toluene is more efficiently transferred to a p-type nanomaterial such as graphene due to better hole mobility. Conversely, MAPbI<sub>3</sub> presents similar mobilities for positive and negative charges, lowering their efficiency.

### 3.4. Potential Use for Breath Analysis

Detection of gases susceptible to be biomarkers of health issues in exhaled breath should overcome a key challenge as was mentioned before. Water vapor is probably the highest cross-interferent molecule present in breath. Moreover, this problem is magnified when using halide perovskites, which experience fast degradation. However, promising results were obtained in a humid atmosphere using graphene loaded with perovskite nanocrystals. Contact angle measurements revealed the highly hydrophobic surface obtained from graphene (Figure 8a) and therefore minimizing the impact of the water molecules on perovskite nanocrystals. Actually, bare graphene tends to show higher sensitivities in humid conditions when electron-withdrawing gases are being detected [139]. The reason is that water molecules are also electron-withdrawing when interacting with the oxygen-containing groups of graphene. As a result, water-mediated adsorption is promoted, inducing larger resistance changes [140]. Conversely, perovskite@graphene nanohybrids show similar responses in dry and humid conditions (Figure 8b). A slight decrease in the sensitivity in the presence of ambient moisture is even observed. The possible reason beyond this sensing mechanism is the partial passivation of perovskite in humid conditions. As a result, the charge transport and the formation of electron–hole pairs are lowered at the perovskite nanocrystals [141].

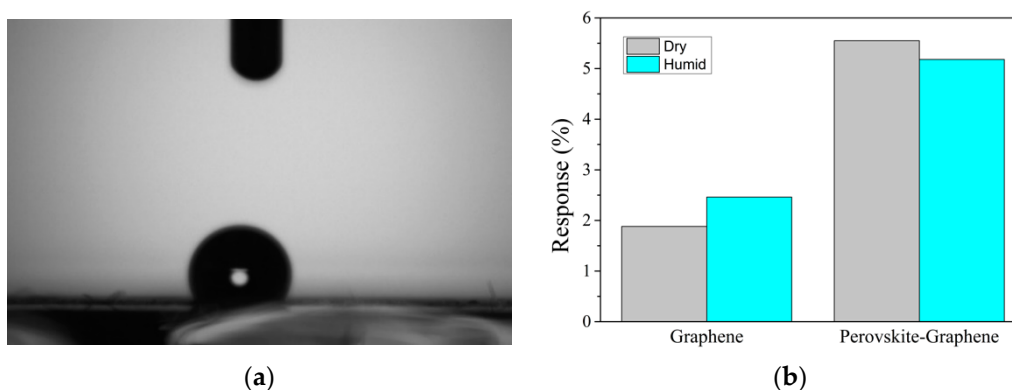


**Figure 8.** (a) Contact angle measurement for graphene loaded with MAPbBr<sub>3</sub> perovskite nanocrystals. Adapted from *Sensors* MDPI. (b) Comparison of the sensing responses for 500 ppm of NO<sub>2</sub> in dry and humid conditions. Reproduced from *Sensors* MDPI 2019, 19 (20), 4563.

These results show an innovative approach to employ perovskites in gas sensing devices operated at room temperature. Thanks to graphene's hydrophobicity, lead halide perovskites are more stable against ambient moisture, thus increasing their stability at least for months. However, further improvements are required to improve the selectivity and optimize the concentrations detected to achieve the trace levels needed for exhaled breath analysis.

#### 4. Conclusions and Outlook

The graphene loading with perovskite nanocrystals has been shown to be a feasible nanomaterial for sensing applications, in which a synergistic effect between both materials is created. The presence of perovskite nanocrystals can easily enhance the reactivity of the sensing layer and therefore ameliorate the poor sensing performance of the bare graphene. The high hydrophobicity that can be achieved via graphene functionalization may protect the perovskites against ambient moisture, which is their main drawback that is preventing their effective use in commercial devices. Moreover, their capability to detect gas molecules at room temperature can pave the way towards low-power consumption and inexpensive devices.

Nevertheless, since few works have reported this approach, more research efforts are needed for elucidating the role and sensing performance of different perovskite compositions. In that way, further optimizations might be performed to improve some sensing parameters, such as reducing the cross-sensitivity or the limit of detection for sensing devices based on perovskite@graphene nanohybrids. In addition, most of the previous works reporting the use of halide perovskites for different applications such as photovoltaics and sensors are based on lead as cation B. However, the use and manipulation of this toxic element can constitute a potential threat to the environment.

Therefore, the recently reported lead-free halide perovskites are a promising nanomaterial for being implemented in gas sensors, opening a potential new research avenue for achieving materials with reduced footprint and toxicity, while outstanding properties can be even further improved in comparison to their lead halide counterparts. In that way, regarding the sensing of gas molecules, perovskite@graphene nanohybrids may be employed in a wide range of applications, such as monitoring ambient pollutants or detecting biomarkers in breath analysis, to cite some.

**Author Contributions:** Conceptualization, J.C.-C., C.B. and E.L.; writing—original draft preparation, J.C.-C. and R.G.-A.; review and supervision, P.A., C.B. and E.L. All authors have read and agreed to the published version of the manuscript.

**Funding:** This research was supported in part by MICINN and FEDER via grants no. RTI2018-101580-B-I00, by AGAUR under grant 2017SGR418 and by Belgian Fund for Scientific Research

under FRFC contract J001019. J.C.C. gratefully acknowledges a postdoctoral fellowship from URV. R.G.A. acknowledges an FPI scholarship from MINECO TEC2015-74405-JIN and MAT2015-69669-P. P.A. acknowledges the financial support from the Spanish Government through “Severo Ochoa” (SEV-2016-0683, MINECO) and PGC2018-099744-B-I00 (MCIU/AEI/FEDER). E.L. is supported by the Catalan institution for Research and Advanced Studies via the 2018 Edition of the ICREA Academia Award. C.B. is a research associate at the National Funds for Scientific Research (FRS-FNRS, Belgium).

**Institutional Review Board Statement:** Not applicable.

**Informed Consent Statement:** Not applicable.

**Data Availability Statement:** Raw data are available from authors upon request.

**Conflicts of Interest:** The authors declare no conflict of interest.

## References

1. Das, S.; Pal, M. Review—Non-Invasive Monitoring of Human Health by Exhaled Breath Analysis: A Comprehensive Review. *J. Electrochem. Soc.* **2020**, *167*, 037562. [[CrossRef](#)]
2. Cikach, F.S.; Dweik, R.A. Cardiovascular Biomarkers in Exhaled Breath. *Prog. Cardiovasc. Dis.* **2012**, *55*, 34–43. [[CrossRef](#)]
3. du Plessis, A.; le Roux, S.G.; Guelpa, A. Comparison of Medical and Industrial X-Ray Computed Tomography for Non-Destructive Testing. *Case Stud. Nondestruct. Test. Eval.* **2016**, *6*, 17–25. [[CrossRef](#)]
4. Mashir, A.; Dweik, R.A. Exhaled Breath Analysis: The New Interface between Medicine and Engineering. *Adv. Powder Technol.* **2009**, *20*, 420–425. [[CrossRef](#)]
5. Radogna, A.V.; Siciliano, P.A.; Sabina, S.; Sabato, E.; Capone, S. A Low-Cost Breath Analyzer Module in Domiciliary Non-Invasive Mechanical Ventilation for Remote Copd Patient Monitoring. *Sensors* **2020**, *20*, 653. [[CrossRef](#)]
6. Grob, N.M.; Aytakin, M.; Dweik, R.A. Biomarkers in Exhaled Breath Condensate: A Review of Collection, Processing and Analysis. *J. Breath Res.* **2008**, *2*, 037004. [[CrossRef](#)] [[PubMed](#)]
7. Dent, A.G.; Sutedja, T.G.; Zimmerman, P.V. Exhaled Breath Analysis for Lung Cancer. *J. Thorac. Dis.* **2013**, *5*, S540.
8. Koureas, M.; Kirgou, P.; Amoutzias, G.; Hadjichristodoulou, C.; Gourgoulanis, K.; Tsakalof, A. Target Analysis of Volatile Organic Compounds in Exhaled Breath for Lung Cancer Discrimination from Other Pulmonary Diseases and Healthy Persons. *Metabolites* **2020**, *10*, 317. [[CrossRef](#)]
9. Beccaria, M.; Bobak, C.; Maitshotlo, B.; Mellors, T.R.; Purcaro, G.; Franchina, F.A.; Rees, C.A.; Nasir, M.; Black, A.; Hill, J.E. Exhaled Human Breath Analysis in Active Pulmonary Tuberculosis Diagnostics by Comprehensive Gas Chromatography-Mass Spectrometry and Chemometric Techniques. *J. Breath Res.* **2019**, *13*, 16005. [[CrossRef](#)]
10. Ribes, A.; Carrera, G.; Gallego, E.; Roca, X.; Berenguer, M.J.; Guardino, X. Development and Validation of a Method for Air-Quality and Nuisance Odors Monitoring of Volatile Organic Compounds Using Multi-Sorbent Adsorption and Gas Chromatography/Mass Spectrometry Thermal Desorption System. *J. Chromatogr. A* **2007**, *1140*, 44–55. [[CrossRef](#)]
11. Sola Martínez, R.A.; Pastor Hernández, J.M.; Lozano Terol, G.; Gallego-Jara, J.; García-Marcos, L.; Cánovas Díaz, M.; de Diego Puente, T. Data Preprocessing Workflow for Exhaled Breath Analysis by GC/MS Using Open Sources. *Sci. Rep.* **2020**, *10*, 1–11. [[CrossRef](#)]
12. Mirzaei, A.; Leonardi, S.G.; Neri, G. Detection of Hazardous Volatile Organic Compounds (VOCs) by Metal Oxide Nanostructures-Based Gas Sensors: A Review. *Ceram. Int.* **2016**, *42*, 15119–15141. [[CrossRef](#)]
13. Meng, F.L.; Guo, Z.; Huang, X.J. Graphene-Based Hybrids for Chemiresistive Gas Sensors. *TrAC Trends Anal. Chem.* **2015**, *68*, 37–47. [[CrossRef](#)]
14. Neri, G. First Fifty Years of Chemoresistive Gas Sensors. *Chemosensors* **2015**, *3*, 1–20. [[CrossRef](#)]
15. Zhang, Z.; Zhang, S.; Jiang, C.; Guo, H.; Qu, F.; Shimakawa, Y.; Yang, M. Integrated Sensing Array of the Perovskite-Type  $\text{LnFeO}_3$  ( $\text{Ln}=\text{La, Pr, Nd, Sm}$ ) to Discriminate Detection of Volatile Sulfur Compounds. *J. Hazard. Mater.* **2021**, *413*, 125380. [[CrossRef](#)] [[PubMed](#)]
16. Zhang, Y.; Zhao, J.; Du, T.; Zhu, Z.; Zhang, J.; Liu, Q. A Gas Sensor Array for the Simultaneous Detection of Multiple VOCs. *Sci. Rep.* **2017**, *7*, 1–8. [[CrossRef](#)]
17. Di Natale, C.; Martinelli, E.; Pennazza, G.; Orsini, A.; Santonico, M. Data Analysis for Chemical Sensor Arrays. In *Advances in Sensing with Security Applications*; Springer: Dordrecht, The Netherlands, 2006; Volume 2, pp. 147–169.
18. Scott, S.M.; James, D.; Ali, Z. Data Analysis for Electronic Nose Systems. *Microchim. Acta* **2006**, *156*, 183–207. [[CrossRef](#)]
19. Buckley, D.J.; Black, N.C.G.; Castanon, E.G.; Melios, C.; Hardman, M.; Kazakova, O. Frontiers of Graphene and 2D Material-Based Gas Sensors for Environmental Monitoring. *2D Mater.* **2020**, *7*, 032002. [[CrossRef](#)]
20. Travan, C.; Bergmann, A.  $\text{NO}_2$  and  $\text{NH}_3$  Sensing Characteristics of Inkjet Printing Graphene Gas Sensors. *Sensors* **2019**, *19*, 3379. [[CrossRef](#)]
21. Rodner, M.; Puglisi, D.; Ekeröth, S.; Helmersson, U.; Shteplyuk, I.; Yakimova, R.; Skallberg, A.; Uvdal, K.; Schütze, A.; Eriksson, J. Graphene Decorated with Iron Oxide Nanoparticles for Highly Sensitive Interaction with Volatile Organic Compounds. *Sensors* **2019**, *19*, 918. [[CrossRef](#)] [[PubMed](#)]

22. Ovsianytskyi, O.; Nam, Y.S.; Tsymbalenko, O.; Lan, P.T.; Moon, M.W.; Lee, K.B. Highly Sensitive Chemiresistive H<sub>2</sub>S Gas Sensor Based on Graphene Decorated with Ag Nanoparticles and Charged Impurities. *Sens. Actuators B Chem.* **2018**, *257*, 278–285. [[CrossRef](#)]
23. Ren, Y.; Zhu, C.; Cai, W.; Li, H.; Ji, H.; Kholmanov, I.; Wu, Y.; Piner, R.D.; Ruoff, R.S. Detection of Sulfur Dioxide Gas with Graphene Field Effect Transistor. *Appl. Phys. Lett.* **2012**, *100*, 163114. [[CrossRef](#)]
24. Panda, D.; Nandi, A.; Datta, S.K.; Saha, H.; Majumdar, S. Selective Detection of Carbon Monoxide (CO) Gas by Reduced Graphene Oxide (RGO) at Room Temperature. *RSC Adv.* **2016**, *6*, 47337–47348. [[CrossRef](#)]
25. Smith, A.D.; Elgammal, K.; Fan, X.; Lemme, M.C.; Delin, A.; Rålander, M.; Bergqvist, L.; Schröder, S.; Fischer, A.C.; Niklaus, F.; et al. Graphene-Based CO<sub>2</sub> Sensing and Its Cross-Sensitivity with Humidity. *RSC Adv.* **2017**, *7*, 22329–22339. [[CrossRef](#)]
26. Cadore, A.R.; Mania, E.; Alencar, A.B.; Rezende, N.P.; de Oliveira, S.; Watanabe, K.; Taniguchi, T.; Chacham, H.; Campos, L.C.; Lacerda, R.G. Enhancing the Response of NH<sub>3</sub> Graphene-Sensors by Using Devices with Different Graphene-Substrate Distances. *Sens. Actuators B Chem.* **2018**, *266*, 438–446. [[CrossRef](#)]
27. Hwang, H.M.; Hwang, E.; Kim, D.; Lee, H. Mesoporous Non-Stacked Graphene-Receptor Sensor for Detecting Nerve Agents. *Sci. Rep.* **2016**, *6*, 33299. [[CrossRef](#)]
28. Yuan, W.; Shi, G. Graphene-Based Gas Sensors. *J. Mater. Chem. A* **2013**, *1*, 10078–10091. [[CrossRef](#)]
29. Araya-Hermosilla, E.; Minichino, M.; Mattoli, V.; Pucci, A. Chemical and Temperature Sensors Based on Functionalized Reduced Graphene Oxide. *Chemosensors* **2020**, *8*, 43. [[CrossRef](#)]
30. Tian, W.; Liu, X.; Yu, W. Research Progress of Gas Sensor Based on Graphene and Its Derivatives: A Review. *Appl. Sci.* **2018**, *8*, 1118. [[CrossRef](#)]
31. Deokar, G.; Casanova-Cháfer, J.; Rajput, N.S.; Aubry, C.; Llobet, E.; Jouiad, M.; Costa, P.M.F.J. Wafer-Scale Few-Layer Graphene Growth on Cu/Ni Films for Gas Sensing Applications. *Sens. Actuators B Chem.* **2020**, *305*, 127458. [[CrossRef](#)]
32. Joshi, N.; Hayasaka, T.; Liu, Y.; Liu, H.; Oliveira, O.N.; Lin, L. A Review on Chemiresistive Room Temperature Gas Sensors Based on Metal Oxide Nanostructures, Graphene and 2D Transition Metal Dichalcogenides. *Microchim. Acta* **2018**, *185*, 1–16. [[CrossRef](#)]
33. Li, Q.; Liu, W.; Cao, G.; Li, X.; Wang, X. A Study of Gas Sensing Behavior of Metal-Graphene Contact with Transfer Length Method. *Appl. Phys. Lett.* **2016**, *108*, 221604. [[CrossRef](#)]
34. Wu, H.; Li, Q.; Bu, X.; Liu, W.; Cao, G.; Li, X.; Wang, X. Gas Sensing Performance of Graphene-Metal Contact after Thermal Annealing. *Sens. Actuators B Chem.* **2019**, *282*, 408–416. [[CrossRef](#)]
35. Pereira, C.L.; Cadore, A.R.; Rezende, N.P.; Gadelha, A.; Soares, E.A.; Chacham, H.; Campos, L.C.; Lacerda, R.G. Reversible Doping of Graphene Field Effect Transistors by Molecular Hydrogen: The Role of the Metal/Graphene Interface. *2D Mater.* **2019**, *6*, 025037. [[CrossRef](#)]
36. Behi, S.; Bohli, N.; Casanova-Cháfer, J.; Llobet, E.; Abdelghani, A. Metal Oxide Nanoparticle-Decorated Few Layer Graphene Nanoflake Chemoresistors for the Detection of Aromatic Volatile Organic Compounds. *Sensors* **2020**, *20*, 3413. [[CrossRef](#)]
37. Dey, A.; Chronos, A.; Braithwaite, N.S.J.; Gandhiraman, R.P.; Krishnamurthy, S. Plasma Engineering of Graphene. *Appl. Phys. Rev.* **2016**, *3*, 021301. [[CrossRef](#)]
38. Cho, B.; Yoon, J.; Lim, S.K.; Kim, A.R.; Kim, D.H.; Park, S.G.; Kwon, J.D.; Lee, Y.J.; Lee, K.H.; Lee, B.H.; et al. Chemical Sensing of 2D Graphene/MoS<sub>2</sub> Heterostructure Device. *ACS Appl. Mater. Interfaces* **2015**, *7*, 16775–16780. [[CrossRef](#)]
39. Zamiri, G.; Haseeb, A.S.M.A. Recent Trends and Developments in Graphene/Conducting Polymer Nanocomposites Chemiresistive Sensors. *Materials* **2020**, *13*, 3311. [[CrossRef](#)]
40. Shellaiah, M.; Sun, K.W. Review on Sensing Applications of Perovskite Nanomaterials. *Chemosensors* **2020**, *8*, 55. [[CrossRef](#)]
41. Zhu, Z.; Sun, Q.; Zhang, Z.; Dai, J.; Xing, G.; Li, S.; Huang, X.; Huang, W. Metal Halide Perovskites: Stability and Sensing-Ability. *J. Mater. Chem. C* **2018**, *6*, 10121–10137. [[CrossRef](#)]
42. Kim, B.J.; Fabbri, E.; Abbott, D.F.; Cheng, X.; Clark, A.H.; Nachttegaal, M.; Borlaf, M.; Castelli, I.E.; Graule, T.; Schmidt, T.J. Functional Role of Fe-Doping in Co-Based Perovskite Oxide Catalysts for Oxygen Evolution Reaction. *J. Am. Chem. Soc.* **2019**, *141*, 5231–5240. [[CrossRef](#)]
43. Fergus, J.W. Perovskite Oxides for Semiconductor-Based Gas Sensors. *Sens. Actuators B Chem.* **2007**, *123*, 1169–1179. [[CrossRef](#)]
44. Akkerman, Q.A.; Rainò, G.; Kovalenko, M.V.; Manna, L. Genesis, Challenges and Opportunities for Colloidal Lead Halide Perovskite Nanocrystals. *Nat. Mater.* **2018**, *17*, 394–405. [[CrossRef](#)]
45. Jellicoe, T.C.; Richter, J.M.; Glass, H.F.J.; Tabachnyk, M.; Brady, R.; Dutton, S.E.; Rao, A.; Friend, R.H.; Credgington, D.; Greenham, N.C.; et al. Synthesis and Optical Properties of Lead-Free Cesium Tin Halide Perovskite Nanocrystals. *J. Am. Chem. Soc.* **2016**, *138*, 2941–2944. [[CrossRef](#)]
46. Volonakis, G.; Filip, M.R.; Haghighirad, A.A.; Sakai, N.; Wenger, B.; Snaith, H.J.; Giustino, F. Lead-Free Halide Double Perovskites via Heterovalent Substitution of Noble Metals. *J. Phys. Chem. Lett.* **2016**, *7*, 1254–1259. [[CrossRef](#)]
47. Kieslich, G.; Sun, S.; Cheetham, A.K. An Extended Tolerance Factor Approach for Organic-Inorganic Perovskites. *Chem. Sci.* **2015**, *6*, 3430–3433. [[CrossRef](#)]
48. Saparov, B.; Mitzi, D.B. Organic-Inorganic Perovskites: Structural Versatility for Functional Materials Design. *Chem. Rev.* **2016**, *116*, 4558–4596. [[CrossRef](#)] [[PubMed](#)]
49. Li, M.; Liu, T.; Wang, Y.; Yang, W.; Lü, X. Pressure Responses of Halide Perovskites with Various Compositions, Dimensionalities, and Morphologies. *Matter Radiat. Extrem.* **2020**, *5*, 18201. [[CrossRef](#)]

50. Zhou, C.; Lin, H.; He, Q.; Xu, L.; Worku, M.; Chaaban, M.; Lee, S.; Shi, X.; Du, M.H.; Ma, B. Low Dimensional Metal Halide Perovskites and Hybrids. *Mater. Sci. Eng. R Rep.* **2019**, *137*, 38–65. [[CrossRef](#)]
51. Baamran, K.S.; Tahir, M. Ni-Embedded TiO<sub>2</sub>-ZnTiO<sub>3</sub> Reducible Perovskite Composite with Synergistic Effect of Metal/Support towards Enhanced H<sub>2</sub> Production via Phenol Steam Reforming. *Energy Convers. Manag.* **2019**, *200*, 112064. [[CrossRef](#)]
52. Yin, Y.; Shen, Y.; Zhou, P.; Lu, R.; Li, A.; Zhao, S.; Liu, W.; Wei, D.; Wei, K. Fabrication, Characterization and n-Propanol Sensing Properties of Perovskite-Type ZnSnO<sub>3</sub> Nanospheres Based Gas Sensor. *Appl. Surf. Sci.* **2020**, *509*, 145335. [[CrossRef](#)]
53. Gildo-Ortiz, L.; Reyes-Gómez, J.; Flores-Álvarez, J.M.; Guillén-Bonilla, H.; Olvera, M. de la, L.; Rodríguez Betancourt, V.M.; Verde-Gómez, Y.; Guillén-Cervantes, A.; Santoyo-Salazar, J. Synthesis, Characterization and Sensitivity Tests of Perovskite-Type LaFeO<sub>3</sub> Nanoparticles in CO and Propane Atmospheres. *Ceram. Int.* **2016**, *42*, 18821–18827. [[CrossRef](#)]
54. Michel, C.R.; Martínez-Preciado, A.H.; López-Mena, E.R.; Elías-Zuñiga, A.; Cayetano-Castro, N.; Ceballos-Sanchez, O. Improvement of the Gas Sensing Response of Nanostructured LaCoO<sub>3</sub> by the Addition of Ag Nanoparticles. *Sens. Actuators B Chem.* **2017**, *246*, 181–189. [[CrossRef](#)]
55. Chen, M.; Zhang, Y.; Zhang, J.; Li, K.; Lv, T.; Shen, K.; Zhu, Z.; Liu, Q. Facile Lotus-Leaf-Templated Synthesis and Enhanced Xylene Gas Sensing Properties of Ag-LaFeO<sub>3</sub> Nanoparticles. *J. Mater. Chem. C* **2018**, *6*, 6138–6145. [[CrossRef](#)]
56. Szafraniak, B.; Fušník, L.; Xu, J.; Gao, F.; Brudnik, A.; Rydosz, A. Semiconducting Metal Oxides: SrTiO<sub>3</sub>, BaTiO<sub>3</sub> and BaSrTiO<sub>3</sub> in Gas-Sensing Applications: A Review. *Coatings* **2021**, *11*, 185. [[CrossRef](#)]
57. Xiao, H.; Xue, C.; Song, P.; Li, J.; Wang, Q. Preparation of Porous LaFeO<sub>3</sub> Microspheres and Their Gas-Sensing Property. *Appl. Surf. Sci.* **2015**, *337*, 65–71. [[CrossRef](#)]
58. Xue, X.Y.; Chen, Y.J.; Wang, Y.G.; Wang, T.H. Synthesis and Ethanol Sensing Properties of ZnSnO<sub>3</sub> Nanowires. *Appl. Phys. Lett.* **2005**, *86*, 1–3. [[CrossRef](#)]
59. Zhang, H.; Yi, J. Enhanced Ethanol Gas Sensing Performance of ZnO Nanoflowers Decorated with LaMnO<sub>3</sub> Perovskite Nanoparticles. *Mater. Lett.* **2018**, *216*, 196–198. [[CrossRef](#)]
60. Sharma, N.; Kushwaha, H.S.; Sharma, S.K.; Sachdev, K. Fabrication of LaFeO<sub>3</sub> and RGO-LaFeO<sub>3</sub> Microspheres Based Gas Sensors for Detection of NO<sub>2</sub> and CO. *RSC Adv.* **2020**, *10*, 1297–1308. [[CrossRef](#)]
61. Mahmoudi, T.; Wang, Y.; Hahn, Y.-B. SrTiO<sub>3</sub>/Al<sub>2</sub>O<sub>3</sub>-Graphene Electron Transport Layer for Highly Stable and Efficient Composites-Based Perovskite Solar Cells with 20.6% Efficiency. *Adv. Energy Mater.* **2020**, *10*, 1903369. [[CrossRef](#)]
62. Ihlefeld, J.F.; Borland, W.J.; Maria, J.-P. Enhanced Dielectric and Crystalline Properties in Ferroelectric Barium Titanate Thin Films. *Adv. Funct. Mater.* **2007**, *17*, 1199–1203. [[CrossRef](#)]
63. Li, W.; Jacobs, R.; Morgan, D. Predicting the Thermodynamic Stability of Perovskite Oxides Using Machine Learning Models. *Comput. Mater. Sci.* **2018**, *150*, 454–463. [[CrossRef](#)]
64. Arandiyán, H.; Wang, Y.; Sun, H.; Rezaei, M.; Dai, H. Ordered Meso- and Macroporous Perovskite Oxide Catalysts for Emerging Applications. *Chem. Commun.* **2018**, *54*, 6484–6502. [[CrossRef](#)]
65. Alharbi, A.A.; Sackmann, A.; Weimar, U.; Bârsan, N. A Highly Selective Sensor to Acetylene and Ethylene Based on LaFeO<sub>3</sub>. *Sens. Actuators B Chem.* **2020**, *303*, 127204. [[CrossRef](#)]
66. Lin, H.J.; Baltrus, J.P.; Gao, H.; Ding, Y.; Nam, C.Y.; Ohodnicki, P.; Gao, P.X. Perovskite Nanoparticle-Sensitized Ga<sub>2</sub>O<sub>3</sub> Nanorod Arrays for CO Detection at High Temperature. *ACS Appl. Mater. Interfaces* **2016**, *8*, 8880–8887. [[CrossRef](#)]
67. Zhang, B.; Lin, H.J.; Gao, H.; Lu, X.; Nam, C.Y.; Gao, P.X. Perovskite-Sensitized β-Ga<sub>2</sub>O<sub>3</sub> nanorod Arrays for Highly Selective and Sensitive NO<sub>2</sub> detection at High Temperature. *J. Mater. Chem. A* **2020**, *8*, 10845–10854. [[CrossRef](#)]
68. Zhang, H.; Qin, H.; Zhang, P.; Hu, J. High Sensing Properties of 3 Wt % Pd-Doped SmFe<sub>1-x</sub>Mg<sub>x</sub>O<sub>3</sub> Nanocrystalline Powders to Acetone Vapor with Ultralow Concentrations under Light Illumination. *ACS Appl. Mater. Interfaces* **2018**, *10*, 15558–15564. [[CrossRef](#)]
69. Queraltó, A.; Graf, D.; Frohnhoven, R.; Fischer, T.; Vanrompay, H.; Bals, S.; Bartaszyte, A.; Mathur, S. LaFeO<sub>3</sub> Nanofibers for High Detection of Sulfur-Containing Gases. *ACS Sustain. Chem. Eng.* **2019**, *7*, 6023–6032. [[CrossRef](#)]
70. Palimar, S.; Kaushik, S.D.; Siruguri, V.; Swain, D.; Viegas, A.E.; Narayana, C.; Sundaram, N.G. Investigation of Ca Substitution on the Gas Sensing Potential of LaFeO<sub>3</sub> Nanoparticles towards Low Concentration SO<sub>2</sub> Gas. *Dalt. Trans.* **2016**, *45*, 13547–13555. [[CrossRef](#)]
71. Cao, E.; Wang, H.; Wang, X.; Yang, Y.; Hao, W.; Sun, L.; Zhang, Y. Enhanced Ethanol Sensing Performance for Chlorine Doped Nanocrystalline LaFeO<sub>3</sub> Powders by Citric Sol-Gel Method. *Sens. Actuators B Chem.* **2017**, *251*, 885–893. [[CrossRef](#)]
72. Cao, E.; Wu, A.; Wang, H.; Zhang, Y.; Hao, W.; Sun, L. Enhanced Ethanol Sensing Performance of Au and Cl Comodified LaFeO<sub>3</sub> Nanoparticles. *ACS Appl. Nano Mater.* **2019**, *2*, 1541–1551. [[CrossRef](#)]
73. Yin, Y.; Li, F.; Zhang, N.; Ruan, S.; Zhang, H.; Chen, Y. Improved Gas Sensing Properties of Silver-Functionalized ZnSnO<sub>3</sub> Hollow Nanocubes. *Inorg. Chem. Front.* **2018**, *5*, 2123–2131. [[CrossRef](#)]
74. Wei, W.; Guo, S.; Chen, C.; Sun, L.; Chen, Y.; Guo, W.; Ruan, S. High Sensitive and Fast Formaldehyde Gas Sensor Based on Ag-Doped LaFeO<sub>3</sub> nanofibers. *J. Alloys Compd.* **2017**, *695*, 1122–1127. [[CrossRef](#)]
75. Tie, Y.; Ma, S.Y.; Pei, S.T.; Zhang, Q.X.; Zhu, K.M.; Zhang, R.; Xu, X.H.; Han, T.; Liu, W.W. Pr Doped BiFeO<sub>3</sub> Hollow Nanofibers via Electrospinning Method as a Formaldehyde Sensor. *Sens. Actuators B Chem.* **2020**, *308*, 127689. [[CrossRef](#)]
76. Teresita, V.M.; Manikandan, A.; Josephine, B.A.; Sujatha, S.; Antony, S.A. Electromagnetic Properties and Humidity-Sensing Studies of Magnetically Recoverable LaMg<sub>x</sub>Fe<sub>1-x</sub>O<sub>3-δ</sub> Perovskites Nano-Photocatalysts by Sol-Gel Route. *J. Supercond. Nov. Magn.* **2016**, *29*, 1691–1701. [[CrossRef](#)]

77. Duan, Z.; Xu, M.; Li, T.; Zhang, Y.; Zou, H. Super-Fast Response Humidity Sensor Based on  $\text{La}_{0.7}\text{Sr}_{0.3}\text{MnO}_3$  Nanocrystals Prepared by PVP-Assisted Sol-Gel Method. *Sens. Actuators B Chem.* **2018**, *258*, 527–534. [[CrossRef](#)]
78. Righettoni, M.; Amann, A.; Pratsinis, S.E. Breath Analysis by Nanostructured Metal Oxides as Chemo-Resistive Gas Sensors. *Mater. Today* **2015**, *18*, 163–171. [[CrossRef](#)]
79. Chen, Q.; Wang, Y.; Wang, M.; Ma, S.; Wang, P.; Zhang, G.; Chen, W.; Jiao, H.; Liu, L.; Xu, X. Enhanced Acetone Sensor Based on Au Functionalized In-Doped  $\text{ZnSnO}_3$  Nanofibers Synthesized by Electrospinning Method. *J. Colloid Interface Sci.* **2019**, *543*, 285–299. [[CrossRef](#)]
80. Correa-Baena, J.P.; Abate, A.; Saliba, M.; Tress, W.; Jesper Jacobsson, T.; Grätzel, M.; Hagfeldt, A. The Rapid Evolution of Highly Efficient Perovskite Solar Cells. *Energy Environ. Sci.* **2017**, *10*, 710–727. [[CrossRef](#)]
81. García, T.; García-Aboal, R.; Albero, J.; Atienzar, P.; García, H. Vapor-Phase Photocatalytic Overall Water Splitting Using Hybrid Methylammonium Copper and Lead Perovskites. *Nanomaterials* **2020**, *10*, 960. [[CrossRef](#)]
82. Peng, Y.; Albero, J.; Álvarez, E.; García, H. Hybrid Benzidinium Lead Iodide Perovskites with a 1D Structure as Photoinduced Electron Transfer Photocatalysts. *Sustain. Energy Fuels* **2019**, *3*, 2356–2360. [[CrossRef](#)]
83. Chen, H.; Zhang, M.; Bo, R.; Barugkin, C.; Zheng, J.; Ma, Q.; Huang, S.; Ho-Baillie, A.W.Y.; Catchpole, K.R.; Tricoli, A. Superior Self-Powered Room-Temperature Chemical Sensing with Light-Activated Inorganic Halides Perovskites. *Small* **2018**, *14*, 1702571. [[CrossRef](#)] [[PubMed](#)]
84. Kakavelakis, G.; Gagaoudakis, E.; Petridis, K.; Petromichelaki, V.; Binas, V.; Kiriakidis, G.; Kymakis, E. Solution Processed  $\text{CH}_3\text{NH}_3\text{Pb}_{1-x}\text{Cl}_x$  Perovskite Based Self-Powered Ozone Sensing Element Operated at Room Temperature. *ACS Sens.* **2018**, *3*, 135–142. [[CrossRef](#)]
85. Zhu, R.; Zhang, Y.; Zhong, H.; Wang, X.; Xiao, H.; Chen, Y.; Li, X. High-Performance Room-Temperature  $\text{NO}_2$  Sensors Based on  $\text{CH}_3\text{NH}_3\text{PbBr}_3$  Semiconducting Films: Effect of Surface Capping by Alkyl Chain on Sensor Performance. *J. Phys. Chem. Solids* **2019**, *129*, 270–276. [[CrossRef](#)]
86. Bao, C.; Yang, J.; Zhu, W.; Zhou, X.; Gao, H.; Li, F.; Fu, G.; Yu, T.; Zou, Z. A Resistance Change Effect in Perovskite  $\text{CH}_3\text{NH}_3\text{PbI}_3$  Films Induced by Ammonia. *Chem. Commun.* **2015**, *51*, 15426–15429. [[CrossRef](#)]
87. Gagaoudakis, E.; Panagiotopoulos, A.; Maksudov, T.; Moschogiannaki, M.; Katerinopoulou, D.; Kakavelakis, G.; Kiriakidis, G.; Binas, V.; Kymakis, E.; Petridis, K. Self-Powered, Flexible and Room Temperature Operated Solution Processed Hybrid Metal Halide p-Type Sensing Element for Efficient Hydrogen Detection. *J. Phys. Mater.* **2020**, *3*, 014010. [[CrossRef](#)]
88. Brintakis, K.; Gagaoudakis, E.; Kostopoulou, A.; Faka, V.; Argyrou, A.; Binas, V.; Kiriakidis, G.; Stratakis, E. Ligand-Free All-Inorganic Metal Halide Nanocubes for Fast, Ultra-Sensitive and Self-Powered Ozone Sensors. *Nanoscale Adv.* **2019**, *1*, 2699–2706. [[CrossRef](#)]
89. Zhuang, Y.; Yuan, W.; Qian, L.; Chen, S.; Shi, G. High-Performance Gas Sensors Based on a Thiocyanate Ion-Doped Organometal Halide Perovskite. *Phys. Chem. Chem. Phys.* **2017**, *19*, 12876–12881. [[CrossRef](#)]
90. Nur'aini, A.; Oh, I. Volatile Organic Compound Gas Sensors Based on Methylammonium Lead Iodide Perovskite Operating at Room Temperature. *RSC Adv.* **2020**, *10*, 12982–12987. [[CrossRef](#)]
91. Jiao, W.; He, J.; Zhang, L. Synthesis and High Ammonia Gas Sensitivity of  $(\text{CH}_3\text{NH}_3)\text{PbBr}_{3-x}\text{I}_x$  Perovskite Thin Film at Room Temperature. *Sens. Actuators B Chem.* **2020**, *309*, 127786. [[CrossRef](#)]
92. Lin, F.; Li, F.; Lai, Z.; Cai, Z.; Wang, Y.; Wolfbeis, O.S.; Chen, X. MnII-Doped Cesium Lead Chloride Perovskite Nanocrystals: Demonstration of Oxygen Sensing Capability Based on Luminescent Dopants and Host-Dopant Energy Transfer. *ACS Appl. Mater. Interfaces* **2018**, *10*, 23335–23343. [[CrossRef](#)]
93. García-Aboal, R.; García, H.; Remiro-Buenamañana, S.; Atienzar, P. Expanding the Photoresponse of Multidimensional Hybrid Lead Bromide Perovskites into the Visible Region by Incorporation of Subphthalocyanine. *Dalt. Trans.* **2021**, *50*, 6100–6108. [[CrossRef](#)] [[PubMed](#)]
94. Kundu, S.; Kelly, T.L. In Situ Studies of the Degradation Mechanisms of Perovskite Solar Cells. *EcoMat* **2020**, *2*, e12025. [[CrossRef](#)]
95. Ava, T.T.; Al Mamun, A.; Marsillac, S.; Namkoong, G. A Review: Thermal Stability of Methylammonium Lead Halide Based Perovskite Solar Cells. *Appl. Sci.* **2019**, *9*, 188. [[CrossRef](#)]
96. Georgakilas, V.; Otyepka, M.; Bourlinos, A.B.; Chandra, V.; Kim, N.; Kemp, K.C.; Hobza, P.; Zboril, R.; Kim, K.S. Functionalization of Graphene: Covalent and Non-Covalent Approaches, Derivatives and Applications. *Chem. Rev.* **2012**, *112*, 6156–6214. [[CrossRef](#)] [[PubMed](#)]
97. Song, S.H.; Park, K.H.; Kim, B.H.; Choi, Y.W.; Jun, G.H.; Lee, D.J.; Kong, B.S.; Paik, K.W.; Jeon, S. Enhanced Thermal Conductivity of Epoxy-Graphene Composites by Using Non-Oxidized Graphene Flakes with Non-Covalent Functionalization. *Adv. Mater.* **2013**, *25*, 732–737. [[CrossRef](#)]
98. Ghosh, A.; Rao, K.V.; George, S.J.; Rao, C.N.R. Noncovalent Functionalization, Exfoliation, and Solubilization of Graphene in Water by Employing a Fluorescent Coronene Carboxylate. *Chem. A Eur. J.* **2010**, *16*, 2700–2704. [[CrossRef](#)]
99. Khan, R.; Nishina, Y. Covalent Functionalization of Carbon Materials with Redox-Active Organic Molecules for Energy Storage. *Nanoscale* **2021**, *13*, 36–50. [[CrossRef](#)]
100. Park, J.; Yan, M. Covalent Functionalization of Graphene with Reactive Intermediates. *Acc. Chem. Res.* **2013**, *46*, 181–189. [[CrossRef](#)]

101. Bottari, G.; Ángeles Herranz, M.; Wibmer, L.; Volland, M.; Rodríguez-Pérez, L.; Guldi, D.M.; Hirsch, A.; Martín, N.; D'Souza, F.; Torres, T. Chemical Functionalization and Characterization of Graphene-Based Materials. *Chem. Soc. Rev.* **2017**, *46*, 4464–4500. [[CrossRef](#)]
102. Hu, C.; Liu, D.; Xiao, Y.; Dai, L. Functionalization of Graphene Materials by Heteroatom-Doping for Energy Conversion and Storage. *Prog. Nat. Sci. Mater. Int.* **2018**, *28*, 121–132. [[CrossRef](#)]
103. Ullah, S.; Shi, Q.; Zhou, J.; Yang, X.; Ta, H.Q.; Hasan, M.; Ahmad, N.M.; Fu, L.; Bachmatiuk, A.; Rummeli, M.H. Advances and Trends in Chemically Doped Graphene. *Adv. Mater. Interfaces* **2020**, *7*, 2000999. [[CrossRef](#)]
104. Ji, X.; Xu, Y.; Zhang, W.; Cui, L.; Liu, J. Review of Functionalization, Structure and Properties of Graphene/Polymer Composite Fibers. *Compos. Part A Appl. Sci. Manuf.* **2016**, *87*, 29–45. [[CrossRef](#)]
105. Pei, S.; Cheng, H.M. The Reduction of Graphene Oxide. *Carbon* **2012**, *50*, 3210–3228. [[CrossRef](#)]
106. Antidormi, A.; Roche, S.; Colombo, L. Impact of Oxidation Morphology on Reduced Graphene Oxides upon Thermal Annealing. *J. Phys Mater.* **2020**, *3*, 15011. [[CrossRef](#)]
107. Alsharaeh, E.; Ahmed, F.; Aldawsari, Y.; Khasawneh, M.; Abuhimd, H.; Alshahrani, M. Novel Synthesis of Holey Reduced Graphene Oxide (HRGO) by Microwave Irradiation Method for Anode in Lithium-Ion Batteries. *Sci. Rep.* **2016**, *6*, 1–13. [[CrossRef](#)] [[PubMed](#)]
108. Li, J.; Qi, X.; Hao, G.; Ren, L.; Zhong, J. In-Situ Investigation of Graphene Oxide under UV Irradiation: Evolution of Work Function. *AIP Adv.* **2015**, *5*, 67154. [[CrossRef](#)]
109. Nakamura, T.; Sato, S. Photochemical Reduction of Graphene Oxide (GO) by Femtosecond Laser Irradiation. In *Laser-based Micro- and Nanoprocessing X*; SPIE: Bellingham, WA, USA, 2016; Volume 9736, p. 973617.
110. Guex, L.G.; Sacchi, B.; Peuvot, K.F.; Andersson, R.L.; Pourrahimi, A.M.; Ström, V.; Farris, S.; Olsson, R.T. Experimental Review: Chemical Reduction of Graphene Oxide (GO) to Reduced Graphene Oxide (RGO) by Aqueous Chemistry. *Nanoscale* **2017**, *9*, 9562–9571. [[CrossRef](#)]
111. Some, S.; Kim, Y.; Yoon, Y.; Yoo, H.; Lee, S.; Park, Y.; Lee, H. High-Quality Reduced Graphene Oxide by a Dual-Function Chemical Reduction and Healing Process. *Sci. Rep.* **2013**, *3*, 1–5. [[CrossRef](#)]
112. Tong, H.; Zhu, J.; Chen, J.; Han, Y.; Yang, S.; Ding, B.; Zhang, X. Electrochemical Reduction of Graphene Oxide and Its Electrochemical Capacitive Performance. *J. Solid State Electrochem.* **2013**, *17*, 2857–2863. [[CrossRef](#)]
113. Chin, S.J.; Doherty, M.; Vempati, S.; Dawson, P.; Byrne, C.; Meenan, B.J.; Guerra, V.; McNally, T. Solvothermal Synthesis of Graphene Oxide and Its Composites with Poly( $\epsilon$ -Caprolactone). *Nanoscale* **2019**, *11*, 18672–18682. [[CrossRef](#)]
114. Dubin, S.; Gilje, S.; Wang, K.; Tung, V.C.; Cha, K.; Hall, A.S.; Farrar, J.; Varshneya, R.; Yang, Y.; Kaner, R.B. A One-Step, Solvothermal Reduction Method for Producing Reduced Graphene Oxide Dispersions in Organic Solvents. *ACS Nano* **2010**, *4*, 3845–3852. [[CrossRef](#)]
115. Song, N.J.; Chen, C.M.; Lu, C.; Liu, Z.; Kong, Q.Q.; Cai, R. Thermally Reduced Graphene Oxide Films as Flexible Lateral Heat Spreaders. *J. Mater. Chem. A* **2014**, *2*, 16563–16568. [[CrossRef](#)]
116. Feng, M.; Feng, H. Effect of Reducing Agent on the Chemical Reduction of Graphene Oxides. *J. Nanosci. Nanotechnol.* **2013**, *13*, 937–941. [[CrossRef](#)]
117. Xie, X.; Zhou, Y.; Huang, K. Advances in Microwave-Assisted Production of Reduced Graphene Oxide. *Front. Chem.* **2019**, *7*, 355. [[CrossRef](#)]
118. Petridis, C.; Kakavelakis, G.; Kymakis, E. Renaissance of Graphene-Related Materials in Photovoltaics Due to the Emergence of Metal Halide Perovskite Solar Cells. *Energy Environ. Sci.* **2018**, *11*, 1030–1061. [[CrossRef](#)]
119. Casanova-Chafer, J.; Garcia-Aboal, R.; Atienzar, P.; Llobet, E. The Role of Anions and Cations in the Gas Sensing Mechanisms of Graphene Decorated with Lead Halide Perovskite Nanocrystals. *Chem. Commun.* **2020**, *56*, 8956–8959. [[CrossRef](#)]
120. Wen, X.; Wu, J.; Gao, D.; Lin, C. Interfacial Engineering with Amino-Functionalized Graphene for Efficient Perovskite Solar Cells. *J. Mater. Chem. A* **2016**, *4*, 13482–13487. [[CrossRef](#)]
121. Li, M.; Zuo, W.W.; Wang, Q.; Wang, K.L.; Zhuo, M.P.; Köbler, H.; Halbig, C.E.; Eigler, S.; Yang, Y.G.; Gao, X.Y.; et al. Ultrathin Nanosheets of Oxo-Functionalized Graphene Inhibit the Ion Migration in Perovskite Solar Cells. *Adv. Energy Mater.* **2020**, *10*, 1902653. [[CrossRef](#)]
122. Butz, B.; Dolle, C.; Halbig, C.E.; Spiecker, E.; Eigler, S. Highly Intact and Pure Oxo-Functionalized Graphene: Synthesis and Electron-Beam-Induced Reduction. *Angew. Chem. Int. Ed.* **2016**, *55*, 15771–15774. [[CrossRef](#)]
123. Wang, Z.; Eigler, S.; Ishii, Y.; Hu, Y.; Papp, C.; Lytken, O.; Steinrück, H.P.; Halik, M. A Facile Approach to Synthesize an Oxo-Functionalized Graphene/Polymer Composite for Low-Voltage Operating Memory Devices. *J. Mater. Chem. C* **2015**, *3*, 8595–8604. [[CrossRef](#)]
124. Enhessari, M.; Salehabadi, A. Perovskites-Based Nanomaterials for Chemical Sensors. In *Progresses in Chemical Sensor*; InTech: London, UK, 2016.
125. Berhe, T.A.; Su, W.N.; Chen, C.H.; Pan, C.J.; Cheng, J.H.; Chen, H.M.; Tsai, M.C.; Chen, L.Y.; Dubale, A.A.; Hwang, B.J. Organometal Halide Perovskite Solar Cells: Degradation and Stability. *Energy Environ. Sci.* **2016**, *9*, 323–356. [[CrossRef](#)]
126. Frost, J.M.; Butler, K.T.; Brivio, F.; Hendon, C.H.; Van Schilfgaarde, M.; Walsh, A. Atomistic Origins of High-Performance in Hybrid Halide Perovskite Solar Cells. *Nano Lett.* **2014**, *14*, 2584–2590. [[CrossRef](#)]

127. Leguy, A.M.A.; Hu, Y.; Campoy-Quiles, M.; Alonso, M.I.; Weber, O.J.; Azarhoosh, P.; Van Schilfhaarde, M.; Weller, M.T.; Bein, T.; Nelson, J.; et al. Reversible Hydration of  $\text{CH}_3\text{NH}_3\text{PbI}_3$  in Films, Single Crystals, and Solar Cells. *Chem. Mater.* **2015**, *27*, 3397–3407. [[CrossRef](#)]
128. Casanova-Cháfer, J.; García-Aboal, R.; Atienzar, P.; Llobet, E. Gas Sensing Properties of Perovskite Decorated Graphene at Room Temperature. *Sensors* **2019**, *19*, 4563. [[CrossRef](#)]
129. Bouclé, J.; Herlin-Boime, N. The Benefits of Graphene for Hybrid Perovskite Solar Cells. *Synth. Met.* **2016**, *222*, 3–16. [[CrossRef](#)]
130. O’Keeffe, P.; Catone, D.; Paladini, A.; Toschi, F.; Turchini, S.; Avaldi, L.; Martelli, F.; Agresti, A.; Pescetelli, S.; Del Rio Castillo, A.E.; et al. Graphene-Induced Improvements of Perovskite Solar Cell Stability: Effects on Hot-Carriers. *Nano Lett.* **2019**, *19*, 684–691. [[CrossRef](#)]
131. Keshavarz, M.; Ottesen, M.; Wiedmann, S.; Wharmby, M.; Küchler, R.; Yuan, H.; Debroye, E.; Steele, J.A.; Martens, J.; Hussey, N.E.; et al. Tracking Structural Phase Transitions in Lead-Halide Perovskites by Means of Thermal Expansion. *Adv. Mater.* **2019**, *31*, 1900521. [[CrossRef](#)] [[PubMed](#)]
132. Meng, Q.; Chen, Y.; Xiao, Y.Y.; Sun, J.; Zhang, X.; Han, C.B.; Gao, H.; Zhang, Y.; Yan, H. Effect of Temperature on the Performance of Perovskite Solar Cells. *J. Mater. Sci. Mater. Electron.* **2020**, *1*, 3. [[CrossRef](#)]
133. Ricciardella, F.; Vollebregt, S.; Polichetti, T.; Miscuglio, M.; Alfano, B.; Miglietta, M.L.; Massera, E.; Di Francia, G.; Sarro, P.M. Effects of Graphene Defects on Gas Sensing Properties towards  $\text{NO}_2$  Detection. *Nanoscale* **2017**, *9*, 6085–6093. [[CrossRef](#)]
134. Garg, R.; Dutta, N.; Choudhury, N. Work Function Engineering of Graphene. *Nanomaterials* **2014**, *4*, 267–300. [[CrossRef](#)]
135. Wang, Y.; Zhang, Y.; Lu, Y.; Xu, W.; Mu, H.; Chen, C.; Qiao, H.; Song, J.; Li, S.; Sun, B.; et al. Hybrid Graphene-Perovskite Phototransistors with Ultrahigh Responsivity and Gain. *Adv. Opt. Mater.* **2015**, *3*, 1389–1396. [[CrossRef](#)]
136. Vickers, E.T.; Graham, T.A.; Chowdhury, A.H.; Bahrami, B.; Dreskin, B.W.; Lindley, S.; Naghadeh, S.B.; Qiao, Q.; Zhang, J.Z. Improving Charge Carrier Delocalization in Perovskite Quantum Dots by Surface Passivation with Conductive Aromatic Ligands. *ACS Energy Lett.* **2018**, *3*, 2931–2939. [[CrossRef](#)]
137. Chen, J.; Messing, M.E.; Zheng, K.; Pullerits, T. Cation-Dependent Hot Carrier Cooling in Halide Perovskite Nanocrystals. *J. Am. Chem. Soc.* **2019**, *141*, 3532–3540. [[CrossRef](#)]
138. Li, X.; Cao, F.; Yu, D.; Chen, J.; Sun, Z.; Shen, Y.; Zhu, Y.; Wang, L.; Wei, Y.; Wu, Y.; et al. All Inorganic Halide Perovskites Nanosystem: Synthesis, Structural Features, Optical Properties and Optoelectronic Applications. *Small* **2017**, *13*, 1603996. [[CrossRef](#)]
139. Lv, C.; Hu, C.; Luo, J.; Liu, S.; Qiao, Y.; Zhang, Z.; Song, J.; Shi, Y.; Cai, J.; Watanabe, A. Recent Advances in Graphene-Based Humidity Sensors. *Nanomaterials* **2019**, *9*, 422. [[CrossRef](#)] [[PubMed](#)]
140. Casanova-Cháfer, J.; Navarrete, E.; Noirfalise, X.; Umek, P.; Bittencourt, C.; Llobet, E. Gas Sensing with Iridium Oxide Nanoparticle Decorated Carbon Nanotubes. *Sensors* **2018**, *19*, 113. [[CrossRef](#)]
141. Fang, H.H.; Adjokatse, S.; Wei, H.; Yang, J.; Blake, G.R.; Huang, J.; Even, J.; Loi, M.A. Ultrahigh Sensitivity of Methylammonium Lead Tribromide Perovskite Single Crystals to Environmental Gases. *Sci. Adv.* **2016**, *2*, e1600534. [[CrossRef](#)]